Department of Applied Physics

Stability Issues of Dye Solar Cells

Muhammad Imran Asghar

Aalto University

DOCTORAL DISSERTATIONS

Aalto University publication series
DOCTORAL DISSERTATIONS 53/2012

Stability Issues of Dye Solar Cells

Muhammad Imran Asghar

Doctoral dissertation for the degree of Doctor of Science in Technology to be presented with due permission of the School of Science for public examination and debate in Auditorium K216 at the Aalto University School of Science (Espoo, Finland) on the 18th of May 2012 at 12 noon.

Aalto University
School of Science
Department of Applied Physics
New Energy Technologies

Supervisor
Prof. Peter Lund

Instructor
D.Sc. Kati Miettunen

Preliminary examiners
Prof. Ronald Österbacka, Åbo Akademi, Finland
D.Sc. Kimmo Solehmainen, VTT Technical Research Centre of Finland

Opponent
Prof. Hironori Arakawa, Tokyo University of Science, Japan

Aalto University publication series
DOCTORAL DISSERTATIONS 53/2012

ISBN 978-952-60-4610-5 (printed)
ISBN 978-952-60-4611-2 (pdf)
ISSN-L 1799-4934
ISSN 1799-4934 (printed)
ISSN 1799-4942 (pdf)

Unigrafia Oy
Helsinki 2012

Finland

The dissertation can be read at http://lib.tkk.fi/Diss/

Publication orders (printed book):
imran.asghar@aalto.fi

Author
Muhammad Imran Asghar

Name of the doctoral dissertation
Stability Issues of Dye Solar Cells

Publisher School of Science

Unit Department of Applied Physics

Series Aalto University publication series DOCTORAL DISSERTATIONS 53/2012

Field of research New Energy Technologies

Manuscript submitted 13 December 2011 **Manuscript revised** 1 February 2012

Date of the defence 18 May 2012 **Language** English

☐ **Monograph** ☒ **Article dissertation (summary + original articles)**

Abstract

The thesis discusses dye solar cells (DSCs) which are emerging as a potential candidate for many applications. The goal of the work was to find more stable and higher performing materials for flexible DSCs, improve understanding of the effects on the DSC stability, and to develop experimental methods that give improved resolution of the degradation mechanisms.

First an intensive critical literature review was done to highlight the important degradation mechanisms in DSCs. It was concluded that techniques giving chemical information are needed to understand the degradation reactions and their effect on electrical performance. It would be advantageous to have methods that enable monitoring chemical changes in operating DSCs, or periodically over their lifetime during accelerated ageing tests. Here the focus was on new and advanced in-situ methods that allow continuous study of the aging of the cells. In this regard, optical techniques such as Raman spectroscopy, newly introduced image processing method and recently introduced segmented cell method were employed to bridge the link between the chemical changes in the DSCs and the standard PV measurement methods. Here for instance the image processing was demonstrated to study the bleaching of electrolyte under ultraviolet and visible light at 85°C. The results obtained with the image processing method and the standard electrical measurements were in agreement and showed that the bleaching of electrolyte was initiated by TiO2 and slowed down by the presence of the dye.

For the roll-to-roll production of DSCs cheap, flexible and stable substrates are required. In this work, a series of metals i.e. StS 304, StS 321, StS 316, StS 316L and Ti were successfully stabilized at the CE of a DSC by using a sputtered Pt catalyst layer that doubled also as a corrosion blocking layer. This work was an important step forward towards stable flexible DSCs.

Finally, the degradation due to the manufacturing step related to the electrolyte filling in the DSC was studied. With the help of recently introduced segmented cell method, it was found the nanoporous film of TiO2 was acting as filter for some of the commonly used electrolyte additives i.e. tBP and NMBI. This resulted in spatial performance variation in the DSC which lead to significant losses in the overall performance (here up to 35 % losses in the up-scaling) and thus it has important implications for large area DSCs.

Keywords degradation, dye solar cell, image processing, Raman, stability

ISBN (printed) 978-952-60-4610-5 **ISBN (pdf)** 978-952-60-4611-2

ISSN-L 1799-4934 **ISSN (printed)** 1799-4934 **ISSN (pdf)** 1799-4942

Location of publisher Espoo **Location of printing** Helsinki **Year** 2012

Pages 162 **The dissertation can be read at** http://lib.tkk.fi/Diss/

Preface

This research work was carried out during 2008-2011 at the New Energy Technologies group (NEW), Department of Applied Physics at School of Science, Aalto University in Finland. The research activities were funded by the Academy of Finland and CNB-E project of the Aalto University research program Multidisciplinary Institute of Digitalization and Energy (MIDE). During the work, I attended various conferences being supported by the Graduate School of Energy Technology and Emil Aaltosen Säätiö.

I thank my supervisor Prof. Peter Lund for providing me the opportunity to conduct research work on dye solar cells in a resilient atmosphere, and for his kind support throughout the work. I also thank my instructor Dr. Kati Miettunen for her kind support and guidance. Then I like to pay special thanks to senior researcher Dr. Janne Halme, whom I admire a lot, for his kind guidance and immense scientific knowledge that helped me in better understanding of my research work. I am grateful to all my other past and present colleagues Prof. Torben Lund, Prof. Reko Leino, Prof. Jouko Korppi-Tommola, Prof. Juha Sinkkonen, Adjunct Prof. Hele Savin, Dr. Antti Haarahiltunen, Dr. Mikko Mikkola, Dr. Minna Toivola, Kerttu Aitola, Paula Vahermaa, Ghufran Hashmi, Henri Vahlman, Janne Patakangas, Simone Mastroianni, Anders Rand Andersen, Nguyen Tuyet Phuong, Anna-Stiina Jaaskelainen, Liisa Antila and Erno Kemppainen for the friendly and cooperative attitude towards me. I also thank the summer and part time working students Armi Tiihonen, Nadia Davouloury, Arnaud Hamon, Sampo Kaukonen, Antti Ruuskanen and Mariko Landstrom for their cooperation and making our time unforgettable.

In my personal life, first of all I thank Almighty Allah who gave me enough strength to do this work and help me in all aspects of my life. Then I thank last Prophet Muhammad (Peace Be Upon Him) for conveying His message from Allah. I also like to thank Pakistan as a country whom I love

from depth of my heart. In my family, first I want to thank my grandparents Syed Abdul Waheed, Sarwari Begum, Muhammad Ashraf and Maqbool Khatoon for their prayers and priceless love. Then I like to thank my parents Dr. Muhammad Asghar and Najma Asghar, who have done so much that life becomes so easy and pleasant for me. All my life, I need your love and prayers without which this life means nothing to me. Then I like to thank my brothers Muhammad Nadeem Asghar, Muhammad Yasir Asghar and Muhammad Zeeshan Asghar for their special kind treatment to their younger brother. I also thank my sisters in law Sobia Nadeem, Sumreen Yasir and Khaula Zeeshan. I also like to thank my cousins Sadia and Bushra for their care and affection which never allowed me to miss a sister in my family. I also like to thank Ayesha for her prayers and understanding. I am also grateful to my uncles and aunts Muhammad Zafar, Muhammad Akhtar and Alam Khatoon. I like to pay special thanks to my nieces and nephews Ali, Haris, Maryam, Fajr, Uzma and Abdullah for their love. Finally, I like to thank Zaina for her prayers and understanding.

I would like to express my special gratitude towards Finland as a country, where I arrived 5 years ago and learnt a lot. I like to thank Finnish people in general for their nice and polite attitude. I like to thank all my friends that I made during my life.

Thank you.

Espoo, December 13th 2011

Muhammad Imran Asghar

Table of contents

List of Publications

This thesis is an introduction to the following original publications:

I Asghar, M.I., Miettunen, K., Halme, J., Vahermaa, P., Toivola, M., Aitola, K., and Lund, P., **Review of stability for advanced dye solar cells**, Energy & Environmental Science **3**, 418-426 (2010). http://dx.doi.org/10.1039/b922801b

II Andersen, A.R., Halme, J., Lund, T., Asghar, M.I., Nguyen, P. T., Miettunen, K., Kemppainen, E., and Albrektsen, O., **Charge Transport and Photocurrent Generation Characteristics in Dye Solar Cells Containing Thermally Degraded N719 Dye Molecules**, The Journal of Physical Chemistry C **115**, 15598-15606 (2011). http://dx.doi.org/10.1021/jp201658j

III Asghar, M.I., Miettunen, K., Mastroianni, S., Halme, J., Vahlman, H., and Lund, P., **In-situ image processing method to investigate performance and stability of dye solar cells**, Solar Energy **86**, 331-338 (2012). http://dx.doi.org/10.1016/j.solener.2011.10.006

IV Asghar, I., Miettunen, K., Mastroianni, S., Halme, J., and Lund, P., **Demonstration of image processing method to investigate performance and stability**, *26th European Photovoltaic Solar Energy Conference, Hamburg, Germany, September 5-9, 2011*, Proceedings of 26th European Photovoltaic Solar Energy Conference, 563-566 (2011). http://dx.doi.org/10.4229/26thEUPVSEC2011-1DV.3.27

V Miettunen, K., Asghar, I., Ruan, X., Halme, J., Saukkonen, T., and Lund, P., **Stabilization of metal counter electrodes for dye solar cells**, Journal of Electroanalytical Chemistry **653**, 93-99 (2011). http://dx.doi.org/10.1016/j.jelechem.2010.12.022

VI Miettunen, K., Asghar, I., Halme, J., and Lund, P., **Improved performance and stability of flexible dye solar cells**, *26th European Photovoltaic Solar Energy Conference, Hamburg, Germany, September 5-9, 2011*, Proceedings of 26th European Photovoltaic Solar Energy Conference, 587-590 (2011). http://dx.doi.org/10.4229/26thEUPVSEC2011-1DV.3.36

VII Miettunen, K., Asghar, I., Mastroianni, S., Halme, J., Piers, R.F. Barnes, Rikkinen, E., O'Regan, B., and Lund, P., **Effect of molecular filtering and electrolyte composition on the spatial variation in performance of dye solar cells**, Journal of Electroanalytical Chemistry **664**, 63-72 (2012). http://dx.doi.org/10.1016/j.jelechem.2011.10.012

Other publications by the author not included in the thesis:

1. Asghar, M.I., Miettunen, K., Halme, J., Toivola, M., Aitola, K., Vahermaa, P., and Lund, P., **Stability issues of improved dye sensitized solar cells**, *24th European Photovoltaic Solar Energy Conference*, Proceedings of 24th European Photovoltaic Solar Energy Conference, 93-96 (2009). http://dx.doi.org/10.4229/24thEUPVSEC2009-1AO.6.5
2. Miettunen, K., Toivola, M., Hashmi, G., Salpakari, J., Asghar, I., and Lund, P., **A carbon gel catalyst layer for the roll-to-roll production of dye solar cells**, Carbon **49**, 528-532 (2010). http://dx.doi.org/10.1016/j.carbon.2010.09.052
3. Hashmi, G., Miettunen, K., Peltola, T., Halme, J., Asghar, I., Aitola, K., Toivola, M., and Lund, P., **Review of materials and manufacturing options for large area flexible dye solar cells**, Renewable and Sustainable Energy Reviews **15**, 3717-3732 (2011). http://dx.doi.org/10.1016/j.rser.2011.06.004
4. M.I. Asghar, I. Hakala, J. Jantunen, H. Kettunen, J. Qi, A. Varpula, K. Güven, I.V. Semchenko, S.A. Khakhomov, R. Gonzalo, E Özbay, V. Podlozny, A. Sihvola, S. Tretyakov, and H. Wallén **Electromagnetic Cloaking with a Mixture of Spiral Inclusions**. Metamaterials 2007, Rome, Italy, 22-26 October 2007, 957-980 (2007).
5. V. Vähänissi, A. Haarahiltunen, M. Yli-Koski, H. Talvitie, M. I. Asghar, and H. Savin, **Effect of oxygen in low temperature boron and phosphorus diffusion gettering of iron in Czochralski-grown silicon**, Solid State Phenomena Vols. **156-158** 395-400 (2010). http://dx.doi.org/10.4028/www.scientific.net/SSP.156-158.395
6. H. Savin, M. Yli-Koski, A. Haarahiltunen, V. Virkkala, H. Talvitie, M. I. Asghar, and J. Sinkkonen, **Gettering in silicon-on-insulator wafers with polysilicon layer**, Material Science and Engineering B, Volumes **159-160**, 259-263 (2009). http:/dx.doi.org/10.1016/j.mseb.2008.12.024
7. H. Talvitie, A. Haarahiltunen, H. Savin, M. Yli-Koski, M. I. Asghar and J. Sinkkonen, **Effect of internal gettering of iron on electrical characteristics of devices**, Material Science and

Engineering B, Volumes **159-160**, 269-273 (2009). http:/dx.doi.org/10.1016/j.mseb.2008.10.048

8. M.I. Asghar, M. Yli-Koski, H. Savin, A. Haarahiltunen, H. Talvitie, and J.Sinkkonen, **Competitive iron gettering between internal gettering sites and boron implantation in CZ-silicon**, Material Science and Engineering B, Volumes **159-160**, 224-227 (2009). http://dx.doi.org/10.1016/j.mseb.2008.12.028
9. A. Haarahiltunen, H. Savin, M. Yli-Koski, H. Talvitie, M. I. Asghar, and J. Sinkkonen, **As-grown iron precipitates and gettering in multicrystalline silicon**, Material Science and Engineering B, Volumes **159-160**, 248-252 (2009). http://dx.doi.org/10.1016/j.mseb.2008.10.053
10. A. Haarahiltunen, H. Talvitie, H. Savin, M. Yli-Koski, M. I. Asghar, and J. Sinkkonen, **Modeling boron diffusion gettering of iron in silicon solar cells** , Applied Physics Letters **92**, 021902 (2008). http://dx.doi.org/10.1063/1.2833698
11. A. Haarahiltunen, H. Talvitie, H. Savin, O. Anttila, M. Yli-Koski, M. I. Asghar, and J. Sinkkonen, **Gettering of iron in silicon by boron implantation**, Journal of Materials Science: Materials in Electronics **19**, 41 (2008). http://dx.doi.org/10.1007/s10854-008-9640-2
12. H. Savin, M. Yli-Koski, A. Haarahiltunen, H. Talvitie, M.I. Asghar and J. Sinkkonen, **Copper induced lifetime degradation is silicon solar cell material**, Proceedings of the 23rd European Photovoltaic Solar Energy Conference, 66-68 (2008). http://dx.doi.org/10.4229/23rdEUPVSEC2008-1AO.5.5
13. A. Haarahiltunen, H. Savin, M. Yli-Koski, H. Talvitie, M.I. Asghar and J., Sinkkonen, **Heterogeneous Iron Precipitation and Gettering in Multicrystalline Silicon**, Proceedings of the 23rd European Photovoltaic Solar Energy Conference, 488-490 (2008). http://dx.doi.org/10.4229/23rdEUPVSEC2008-1CV.2.13
14. A. Haarahiltunen, H. Talvitie, H. Savin, M. Yli-Koski, M. I. Asghar, and J. Sinkkonen, **Modeling boron diffusion gettering of iron in silicon solar cells** , Applied Physics Letters **92**, 021902 (2008). http://dx.doi.org/10.1063/1.2833698

Author’s contribution

I: The author is mainly responsible for all parts of this work and writing of the paper. He planned the research work, conducted an intensive literature review on the current state of the art of stability and critically studied the hypothesis related to the degradation mechanisms reported in the literature. Experimental methods and procedures are suggested by the author to effectively study various degradation mechanisms mostly with the help of newly introduced segmented cell method.

II: The author participated in planning of the research work and experimental work. The author was mainly responsible for carrying out Raman spectroscopy and helped in other measurements such as current voltage measurements under 1 Sun. He also contributed in analyzing the measurement results and in writing the paper.

III: The author is mainly responsible for the all parts of this work and writing of the paper. He planned the research work and designed a new measurement method based on image processing techniques and photography. He performed the experimental work and conducted the measurements. He analyzed the measurements results and drew the conclusions.

IV: The author is mainly responsible for all parts of this work and writing of the paper. He planned the experimental work and performed all the experimental and measurements. He analyzed the measurement results and drew the conclusions.

V: The author participated in planning of the work and in conducting the experimental work. He helped in analyzing the measurement results and also contributed in the writing process.

VI: The author participated in planning of the work. He helped in analyzing the measurement results.

VII: The author contributed mainly in the experimental work and the measurements specially the Raman spectroscopy. He also helped in planning the research work and analyzing the measurement results. The author also contributed in writing the paper.

Abbreviations and symbols

Abbreviations

AC	alternating current
ACN	acetonitrile
AM1.5G	air mass 1.5 global
ASTM	American Society for Testing and Materials
BIPV	building integrated photovoltaics
CB	conduction band
CdTe	cadmium telluride
CE	counter electrode
CNT	carbon nanotube
CO	contact
COL	(electron) collection
CPE	constant phase element
CT	charge transfer
$CuInGa(Se)_2$	copper indium gallium selenide
DC	direct current
dcbpy	dicarboxybipyridine
DSC	dye solar cell
EDX	energy dispersive X-ray spectroscopy
EIS	electrochemical impedance spectroscopy
EU	European Union
FTIR	Fourier transform infrared
FTO	fluorine doped tin oxide
Gu	guanidium
HOMO	highest occupied molecular orbital
HSE	high stability electrolyte

HTM	hole transparent material
I^-	iodide ion
I_3^-	tri-iodide ion
IEC	international electrotechnical commission
IEA	international energy agency
IPCC	intergovernmental panel on climate change
IPCE	incident-photon-to-collected-electron efficiency
ITO	indium-tin-oxide
I-V	current-voltage
LUMO	lowest unoccupied molecular orbital
MOS	metal oxide semiconductor
MPN	methoxypropionitrile
MPP	maximum power point
MS	mass spectroscopy
NIR	near infrared
NMBI	N-methylbenzimidazole
OC	open circuit
PE	photoelectrode
PEN	polyethylenenaphthalate
PET	polyethlyeneterephtalate
PMII	1-propyl-3-methylimidazolium iodide
PV	photovoltaic; photovoltaics
R	resistor
redox	reduction-oxidation
RGB	red, green, blue
RT	room temperature
S	series
SC	short circuit
SCN	thiocyanate
SEM	scanning electron microscopy
SRC	standard reporting conditions
StS	stainless steel
SU	substrate
TCO	transparent conductive oxide
UV	ultraviolet
VN	valeronitrile
4-tBP	4-tert-butylpyridine

Symbols

c	speed of light (m/sec)
C	concentration (mol/dm^3)
D	diffusion coefficient (of electrons), (m^2/s)
d	thickness; photoelectrode film thickness, (m)
e^-	electron
E	energy, (J)
f	frequency, (Hz)
F	Faraday's constant
FF	fill factor, (no units)
h	Plank constant
i	current density, (A/m)
I_o	intensity of the incident laser beam
k	index of resistance component
$K(\nu)$	frequency dependent terms
P	power density, (W/m^2)
q_e	elementary charge, (C)
R	reflectance (%); resistance (per unit area) (Ωm^{-2})
S	sensitizer
S^*	excited sensitizer
S^+	oxidized sensitizer
t	time, (s)
T	transmittance, (%)
ν	Raman shift (cm^{-1})
V	voltage, (V)
Z	impedance (per unit area), (Ωm^2)
Φ	photon flux (m^{-2}s^{-1})
η	efficiency, (%)
λ	light wavelength, (m)
τ	time constant, (s)

1. Introduction

1.1. Overview

Life is all about energy handling as all living creatures use energy to maintain their life. Humans like other living creatures consume energy. With increasing human population and change in human lifestyle the consumption of energy increases every year. By the year 2011, the global energy demand is about 13TW [1] which is expected to be 16 TW by the year 2030. Currently, 85% of the needs are fulfilled by fossils fuels [1] which results in carbon emission into the atmosphere. It results in global warming which is big challenge to the society now. According to Intergovernmental panel on climate change (IPCC), 60-80% reduction in the carbon emission is needed by year 2020 in order to limit the climate change [2]. It stresses towards acquiring clean energy and its efficient use. European Union (EU) sets some objectives for energy technology [3] which includes lowering the price of clean energy and putting EU industry at forefront of low carbon emission technology.

German physicist Hermann Von Helmholtz calculated the time for which Sun can provide energy to the Earth and found it to be order of 20 million years approximately [4], hence it can be regarded as an unlimited source of energy. This renewable energy source can provide more than the required energy to fulfill the world's energy needs. Statistics show that in just a couple of hours enough sunlight falls on the Earth's surface to meet the whole world's energy needs for one year [5]. International Energy Agency (IEA) predicted that by the year 2060, the solar energy would meet half of the world's energy demand and most of the world's electricity demand [6]. Approximately two billion people in the world are living without electricity [5]. There are no grid connections to most of such places; hence conventional electricity sources are not useful. However, the Sun shines to most of such places. It shows the potential and bright future of solar energy.

There are two ways to utilize the solar energy i.e. by converting it to thermal energy or to electric energy. A device or tool that converts the light energy directly into electric energy is known as photovoltaic cell. If the source of the light is sun, then it is usually called a solar cell. Photovoltaics generate electricity in a clean and silent way with no moving parts. They have aesthetic value as well. They are widely seen as reliable, sustainable, natural and environmentally friendly energy technology. The photovoltaic market is exponentially growing every year. In year 2010, the annual production of photovoltaic cells reached 23.5 GW [7].

Several types of solar cells exist today. The so called first generation conventional crystalline silicon solar cells are still dominating the PV market by over 85% [7]. The mono-crystalline silicon solar cells have achieved around 27.6% [7] efficiency which is very close to the theoretical limit for silicon solar cells. However, these types of cells require very high quality of crystalline silicon which usually requires expensive processing in the clean rooms which adversely affect the price of the end product. This led the researchers to think of using multi-crystalline silicon solar cells which is much cheaper than mono-crystalline silicon but with reduced efficiencies i.e. 20.4% [7]. However, these cells are still very expensive due to the amount of material used i.e. the thickness of wafers (200 micrometer). This led to the thin film solar cells which are often regarded as second generation of solar cells. It includes cadmium telluride (CdTe), copper indium gallium selenide ($CuInGa(Se)_2$) and amorphous silicon. The cost of these types of cells is much lower than first generation cells, however, stability and lower performance are the main issues to these type of solar cells. The third generation of solar cells includes multi-junction solar cells, organic solar cells and dye solar cells. Multi-junction solar cells, which use multiple junctions to increase the absorption of the sunlight, have achieved the record efficiencies of 43.5% [7]. They are, however, the most expensive solar cells among all types. Both the dye solar cells and the organic solar cells are aiming for low cost with additional features such as flexibility of the cells and feasibility large scale roll to roll production. The highest efficiency for the organic cells is 8.6% [7] whereas dye solar cells have achieved around 12.3% efficiency [9]. Dye solar cells (DSCs) offer a lot of features such as variety of colors, usage of easy available non-toxic

materials, flexibility of substrates, feasibility for large scale roll-to-roll production, and efficient working under low light intensities.

The fate of a certain type of solar cell depends primarily on its performance, life time and cost. Other fundamental factors include availability and non-toxicity of materials, and compatibility with the technological facilities needed to manufacture them. Most importantly, it depends on the final application to which the solar cell is installed.

1.2. Background and scope

The main advantage of the DSCs is that they can provide cheaper electricity as compared to the conventional crystalline silicon solar cells due to usage of cheap materials, simple and easy manufacturing methods, and feasibility for large scale roll-to-roll mass production on flexible substrates [10]. Specially, the possibility of being flexible, acquiring a variety of colors, usage of non-toxic materials and possibility of low weight makes them ideal choice for the building integrated photovoltaics (BIPV). However, commercialization of this technology requires long term stability which is still a challenge for this technology. To overcome this hindrance, a systematic study to understand the degradation mechanisms of DSCs is needed.

Traditionally, DSCs are made on glass based substrates which are on one side coated with a transparent conducting oxide (TCO). Although in most electronics industry indium doped tin oxide (ITO) is used as TCO, due to the high temperature thermal treatments fluorine doped tin oxide (FTO) is commonly used in the traditional DSCs. According to an estimate about 60% of the total material cost of DSCs consists of these TCO glasses [11]. One way to decrease the cost of DSCs is to use cheap metal substrates [10]; however, there are some chemical stability issues involved. The other possibility to decrease the price by using TCO coated plastic substrates coated with the advantage that they can be mass produced using roll-to-roll production. However, the ideal solution would be the complete removal of the TCO from the substrates. Similarly, other expensive components of a DSC such as platinum catalyst and dye can be replaced with cheaper

options. One big challenge in all these efforts to bring the costs of DSCs down is their effect on the stability of the DSC.

The goal of this research work is to improve the stability of the DSCs. For this purpose, the first step is to develop better understanding of the degradation modes in DSCs and to use easy and fast methods to thoroughly study the degradation mechanisms in-situ. For the up-scaling of the DSCs, it is essential to resolve degradation issues related to the cheap flexible metal substrates in DSCs and other degradation issues originated from the manufacturing processes. In order to realize commercialization, a DSC needs to demonstrate high performance at low cost for long term operation. Hence, the materials used in the DSC should be cheap and feasible for roll-to-roll manufacturing at the same time, and the DSCs should be stable for long term operation.

In this research work, a thorough literature review is done to find out the current state of the art of stability of DSCs. It was found that there are no defined standards to test the stability of DSCs. However, there are some commonly used tests which come from thin film solar cells such as light soaking and thermal tests. In addition, it was found that there are several degradation mechanisms reported in the literature regarding the degradation of DSCs which need further investigation. Therefore, during this research work several important degradation processes were investigated such as dye degradation, electrolyte bleaching, stability of catalyst layers, and ageing of metal based DSCs. In addition, a novel in situ method based on visual analysis was introduced to study the performance and stability of DSCs. Furthermore, the performance degradation due to the spatial distribution of the additives in the electrolyte during the electrolyte filling step in the cell preparation is studied in this work.

1.3. Outline of the thesis

The thesis is organized in five chapters followed by the appendix and the original publications. The content of these chapters are as follows:

The Chapter 1 introduces the motivation and the scope of this thesis and also gives a brief background of the studies.

The Chapter 2 covers the basic structure and functioning of dye solar cells. It also includes the performance parameters of the cells and their preparation in the laboratory.

The Chapter 3 deals with the measurements methods and techniques that have been used in the research. A brief introduction to the measurement techniques is given and their application on the dye solar cells is discussed.

The Chapter 4 is comprised of main results of the research work done in this thesis, reported originally in the Publications I-VII. The results are summarized and thoroughly discussed.

The Chapter 5 is about the key findings in the research work and important conclusions made on the basis of those findings. The contributions and implications of this thesis to the field of dye solar cells are discussed.

The original Publications I-VII are reproduced at the end of the thesis with the kind permission from the copyright holders.

2. The dye solar cell

2.1. Dye solar cell structure

Dye solar cell (DSC) comprises of a photo-electrochemical device consisting of a photoelectrode (PE), hole transparent material (HTM) i.e electrolyte and a counter electrode (CE) sandwiched together. The schematic of the structure of a DSC is shown in the Figure 1.

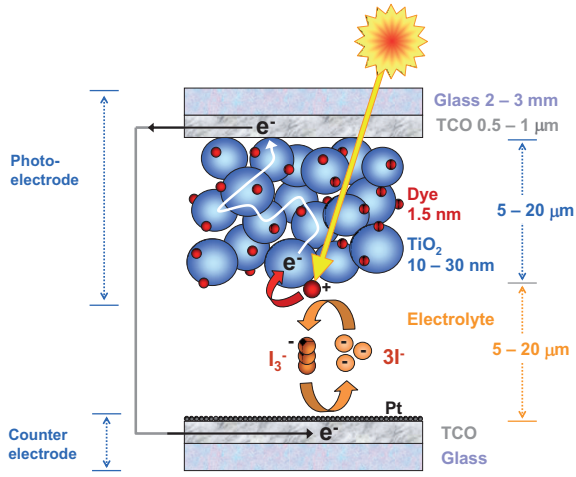

Figure 1. The schematics of structure of a DSC [12]

The photoelectrode consists of a nanoporous film of a semiconductor oxide usually TiO_2 (5-20 μm thick) sensitized with a monolayer of a photo sensitive dye, deposited on a TCO coated substrate. The most common dye used in DSC is hydrophilic red dye (*cis*-bis (isothiocyanato) bis(2,2'-bipyridyl-4,4'-dicarboxylato)-ruthenium(II)bis-tetrabutylammonium) which is usually referred as N719. In conventional glass based DSCs, the TCO is composed of FTO and substrate is rigid glass. In flexible DSCs based on plastic substrates such as polyethyleneterephalate (PET) and

polyethylenenaphthalate (PEN), ITO is used as TCO [13,14,15,16]. To achieve a good conduction of the electrons through the nanoporous film of TiO_2, the film is sintered at 450-500 °C for approximately 30 minutes. This treatment improves the contact between the nano particles and also burns out the solvents of the TiO_2 paste as well as organic impurities. However, in the case of plastic based DSCs, the temperature treatments are limited to 150 °C. Therefore, other techniques such as pressing [13,14] and laser or ultra violet treatments [15,16] have been also applied to improve the contact between the TiO_2 particles. Generally, the quality of nanoporous films is better in glass based DSCs than plastic based DSCs. Fortunately, many flexible metal based photoelectrodes can be sintered at the same high temperatures as in the case of glass based photoelectrodes [17,18,19]. Hence, high quality nanoporous TiO_2 films can be achieved in metal based DSCs.

The HTM can be a solid or liquid state electrolyte. Liquid electrolytes having iodide/tri-iodide redox couple as a redox mediator are mostly being used as HTM in the DSC. The common solvents in the electrolytes includes 3-methoxypropionitrile (MPN) and a mixture of acetonitrile:valeronitrile (ACN:VN). However, MPN is preferred over ACN:VN due to its non-toxicity and higher boiling point to reach better stability [20]. The boiling point of MPN is 164-165 °C whereas that of ACN is only 81-82 °C. Two important factors that need to be considered in the case of liquid electrolyte are the sufficient vapor pressure (volatility) to reach good stability and low viscosity of a liquid electrolyte to get good performance. Another type of electrolytes based on ionic liquid has been used in DSCs due to its non-volatility and excellent stability [21,22,23]. However, the limiting factor for such electrolytes may be their high viscosity causing sluggish charge transfer [20].

The counter electrode is composed on a substrate coated with a TCO layer and a catalyst layer. The commonly used substrate is FTO-glass. In plastic based DSCs, mostly it is PET or PEN with ITO coating. Typically the catalyst film is composed of a few nanometers of Pt particles. There are several ways to deposit Pt on glass or plastic substrate such as thermal platinization [24,25], sputtering [26,27], chemical deposition [28,29], and electrochemical deposition [19,24,30,31]. Another catalyst material that has been used is carbon. As the catalytic properties of carbon are not as good as

those of Pt, a thicker layer of few micrometers is required to achieve the same catalytic properties [32,33]. Thermal platinization has been the most stable option so far [21-25], however, it requires a high temperature treatment step at 385 °C for 20 minutes. Therefore, that method cannot be applied on plastics and alternative low temperature treatments such as sputtering are required. Some metal substrates could endure the high temperature treatment but typically better performance is gained with low temperature treatments e.g. sputtering as shown e.g. in Publication V.

2.2. Working principle of dye solar cells

In this section the working principle of a DSC is thoroughly explained with the help of the Figure 2.

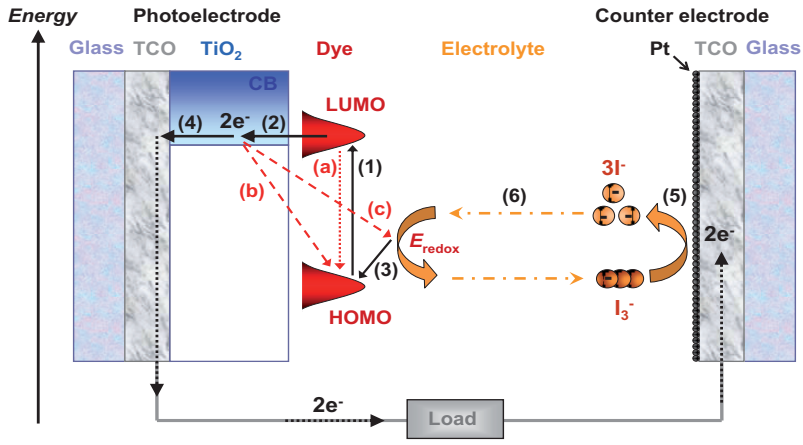

Figure 2. The schematic is showing the working principle of a DSC including all the steps and reactions involved during a complete working cycle and the energy levels in the process [12].

When the light falls on a DSC, the photosensitive dye absorbs the light and gets into an excited state by the electrons jumping from the highest occupied molecular orbital (HOMO) to the lower unoccupied molecular orbital (LUMO) as shown in the step 1 in the Figure 2. The dye immediately

injects the electrons into the conduction band of the TiO_2 and attains oxidized state as shown in step 2. The oxidized state is reduced by the iodide in the electrolyte which in turn gets oxidized to tri-iodide as shown in the step 3. The tri-iodide is transported to the CE through the electrolyte layer. On the other side, the injected electrons are diffused through the TiO_2 film to the TCO layer from where they move through the external load and reach the other side of the DSC i.e. CE as marked as step 4 in the Figure 2. At the CE, the tri-iodide is reduced to iodide as shown as step 5. The dye is ready to absorb new photons and the iodide generated at the CE is ready to regenerate the oxidized dye as shown in the step 6 as shown in the Figure 2. Those electrons in the LUMO which fail to transfer to the conduction band of TiO_2, may drop to the HOMO as shown in process (a) in the Figure 2. Similarly, the electrons in the conduction band may be recombined with the dye or the electrolyte as shown in the process (b) and (c) respectively in the Figure 2.

2.3. Degradation of dye solar cells

Degradation can be defined as loss of performance with the passage of time. The degradation may be permanent (irreversible) or temporary (reversible). During the last two decades, several degradation mechanisms have been reported in the literature (Publication I & II) under different conditions leading to the partial or complete loss of the performance of DSCs. Sometimes degradation occurred due to chemical instability of the materials (Publication V & VI), sometimes it occurred due to the stress factors such as temperature, humidity, ultraviolet and visible light intensity (Publication III & IV). Both stable and unstable results have been reported in the literature using different materials prepared with different manufacturing methods (Publication I). Lots of materials have been used in a DSC at different locations i.e. at PE, at CE or in the electrolyte. The stability data suggests that it is the right combination of materials at the right place that leads to the long term stability for DSCs [21,22,23,46].

The stability of DSCs can be further divided into extrinsic and intrinsic stability. The extrinsic stability includes the sealing issues. Good extrinsic stability is essential to study the intrinsic stability. The intrinsic stability

deals with the degradation mechanisms inside a DSC and their effect on the stability of the device i.e. DSC.

The manufacturing methods also play an important role on the stability of DSCs, as the same material prepared with different manufacturing methods have been shown different stability (Publication V). For instance, thermally platinized has shown better stability as compared to sputtered Pt at the CE on the glass based DSC at 80°C [54], whereas sputtered Pt showed better stability results as compared to thermally platinized at the CE on a metal based DSC (Publication V&VI).

The state of the art of stability of DSC is that rigid glass based DSC have been demonstrated as stable under light soaking tests at 60°C and thermal tests at 80°C for 1000 hours (Table 4). However, the flexible DSCs based on plastic and metals have been stable under light soaking at RT (Publication V) and stability at 80°C for 1000h has not been achieved yet. No DSC has yet passed light soaking test at 80°C for 1000 hours.

3. Measurement techniques and methods

The aim of this chapter is to familiarize the measurement techniques and methods that were used in this work. Some of the measurement techniques are fundamental and are routinely used in the evaluation of the performance of a solar cell such as I-V measurements under 1 Sun, electrochemical impedance spectroscopy (EIS) and incident-photon-to-collected-electron efficiency (IPCE). There are also other methods which are specifically applied to study a particular phenomenon in the device such as Raman spectroscopy, segmented cell method and image processing method. To effectively study the degradation mechanisms in DSCs, techniques giving chemical information are needed. Unfortunately most of the chemical techniques such as mass spectroscopy (MS) require disassemble of the DSC which is hampering their use as a standard PV technique. However, chemical information can be obtained by using the standard PV methods and some other methods such as Raman spectroscopy and image processing method after finding a relationship of the chemical changes in DSCs with these techniques. This way the degradation reactions may be studied using the in-situ measurement methods. The Figure 3 shows the measurement techniques used in this work and are categorized as destructive and non-destructive. Some of these techniques are discussed in later sections.

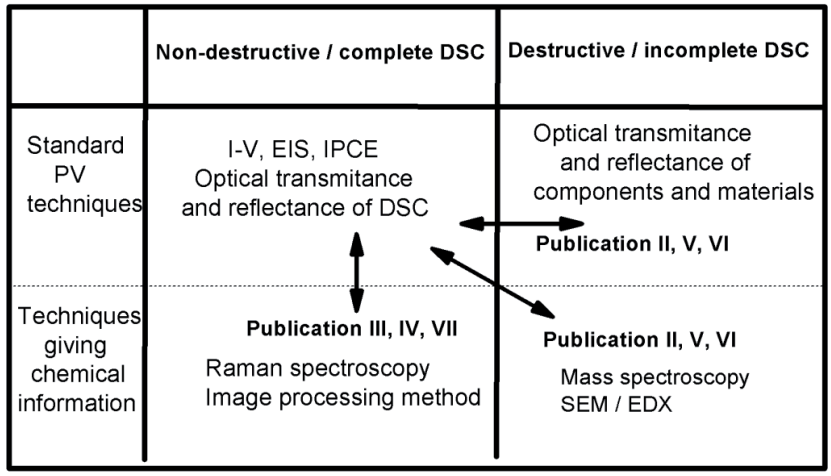

Figure 3. The measurements techniques used in this work categorized as destructive and non-destructive. The arrows are pointing to show that in respective publications these measurements are used together with standard PV measurement techniques.

3.1. I-V under 1 Sun

The performance of a solar cell is usually expressed in terms of its efficiency of converting light energy into electricity. The standard way to measure the efficiency of solar cells is by measuring its current-voltage (I-V). Generally, I-V measurements are performed in a solar simulator in standard reporting conditions (SRC) e.g. 1000 W/m^2 of light intensity with spectrum of air mass 1.5 global (AM1.5G) at 25°C. This standard condition is also referred as 1 Sun. An example of I-V curve of a solar cell is shown in the Figure 4.

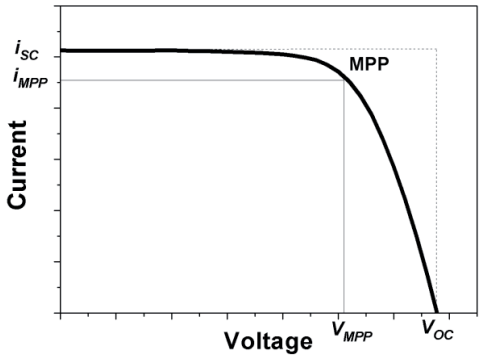

Figure 4. Typical I-V curve of a solar cell and its characteristic parameters

The important characteristic parameters include short circuit current density (i_{SC}), open circuit voltage (V_{OC}), and fill factor (*FF*). The *FF* is defined as

$$FF = \frac{V_{MPP}\ i_{MPP}}{V_{OC}\ i_{SC}} \qquad (1)$$

where i_{MPP} and V_{MPP} are the current density and voltage at the maximum power point (MPP) respectively. The maximum power per unit area delivered by the solar cell is given by

$$P_{MAX} = V_{MPP}\ i_{MPP} \qquad (2)$$

Therefore, in terms of basic characteristic parameters, the maximum power for unit area can be expressed as

$$P_{MAX} = V_{OC}\ i_{SC}\ FF \qquad (3)$$

The efficiency of a solar cell is defined as the ratio of the maximum power produced by the cell (W/m²) to the power of the incident light P_{IN} (W/m²).

$$\eta = \frac{P_{MAX}}{P_{IN}} \qquad (4)$$

Finally in terms of characteristic parameters, the efficiency of a solar cell is given as

$$\eta = \frac{V_{OC}\ i_{SC}\ FF}{P_{IN}} \qquad (5)$$

3.2. Electrochemical impedance spectroscopy

Electrochemical impedance spectroscopy (EIS) is used to study the impedances occurring at different components and their interfaces in a device, here DSC, during its operation. The different components of DSCs have different time constants and thus their impedance response appears at different frequencies which can be studied by scanning a range of frequencies. Before an EIS measurement, DSC is set to steady state operating condition on the I-V curve. During the measurement, the DSC is perturbed with an AC voltage superimposing the DC voltage (operating condition) and the resulting AC current is measured for a certain frequency range. This gives the impedance response of the DSC. The impedance response of the DSC can be understood by fitting the equivalent circuit model for DSC which is shown in the Figure 5 to the measured EIS spectrum.

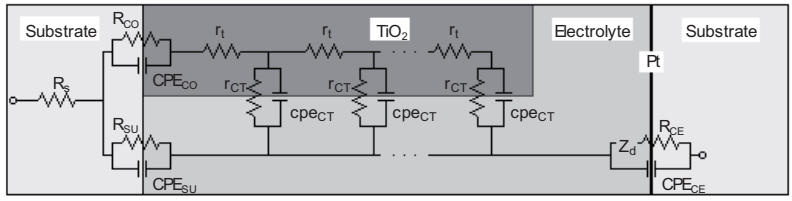

Figure 5. Equivalent circuit model of a DSC [17,34,35,36]. Figure from Publication V.

The equivalent circuit model parameters are as follow:

- R_S is the ohmic series resistance. It is the sum of the contributions from sheet resistance of the substrates (dominant factor), resistivity of the electrolyte, electrical contacts and external wiring.
- R_t (= $r_t d$) is the total electron transport resistance in the TiO_2 film. r_t is the resistivity of the electron transport in the TiO_2 film and d is the thickness of the TiO_2 film.
- Z_d is the mass transport impedance at the counter electrode caused by ionic diffusion in the electrolyte.
- There are also several constant phase element (*CPE*) / resistor (*R*) pairs which are related to different interfaces denoted in the subscript: *SU* the PE substrate / electrolyte, *CO* the PE substrate / the porous TiO_2, *CT* the TiO_2 / electrolyte interface, and *CE* the counter electrode/electrolyte. *CPE* represents a realistic electrode with an uneven and porous surface instead of a pure idealistic capacitor. R is the charge transfer resistance at the interface.

The impedance spectroscopy data are presented in Nyquist and Bode plots. In Nyquist plot, the real and imaginary parts of the impedance at each frequency are plotted in complex planes. In Bode plot, the real and imaginary parts are plotted separately as a function of frequency. A Nyquist plot of a typical impedance response of a DSC gives at high negative voltages two arcs as shown in the Figure 6a. In Bode plot it gives two peaks at high negative voltage as shown in the Figure 6b. Generally at high negative voltages, one arc in the Nyquist plot and one peak in the Bode plot is a result of the R_{CE} and CPE_{CE} pair (in Figure 6 at about 1 kHz). Similarly, at high negative voltages, other arc in Nyquist plot and other peak in Bode plot is a result of R_{CT} and CPE_{CT} pair (in Figure 6 at about 10 Hz). Sometimes at high negative voltages Z_d giving a Warburg element appears (in Figure 6 at about 10 Hz) and it is mostly overlapped with the R_{CT} and CPE_{CT} pair (in Figure 6a&b). The value of R_S can be obtained from the Nyquist plot by the real axis value at the point where the left most arc begins.

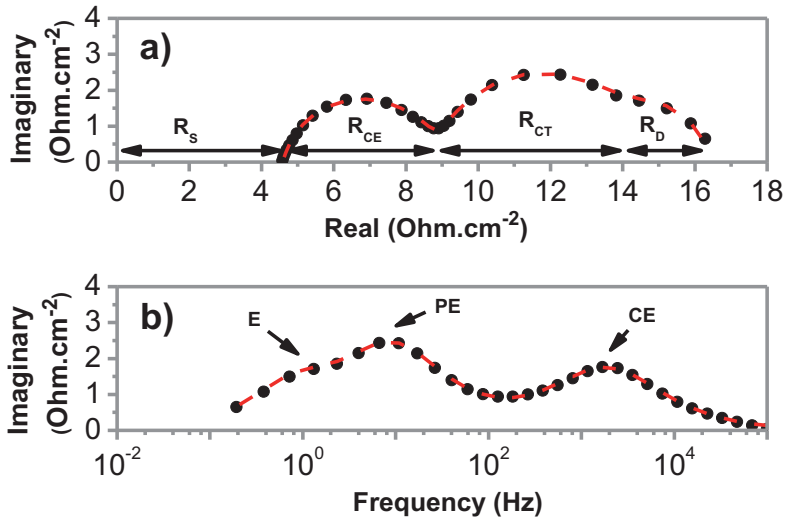

Figure 6. EIS response of a DSC a) a Nyquist plot: real and imaginary part vs frequency (100 mHz – 100 kHz) b) Bode plot: imaginary impedance vs. frequency.

Usually EIS is measured in dark as a function of external voltage to get a broader view of the performance of the individual components in a DSC. In stability studies usually the aged cells show lower R_{CT} and higher CPE_{CT} at a certain voltage compared to their initial state as shown in the Figure 7a&b. In order to study the performance of light independent series connected components of a DSC such as R_S and R_{CE}, measurements done at the same current conditions can be quantitatively compared [12,17]. The easiest way to do this is to carry out the measurements at the open circuit conditions under illumination as done in Publication V.

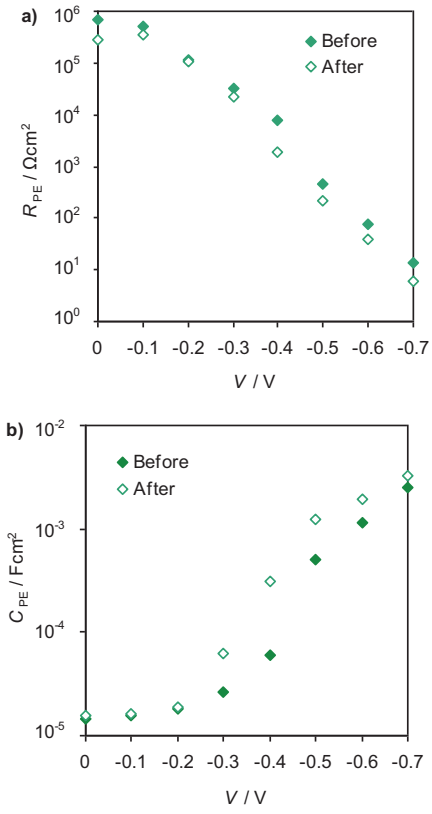

Figure 7. a) Resistance R_{PE} and b) capacitance C_{PE} caused by the parallel connected TiO_2 / electrolyte and PE substrate / electrolyte interfaces in a DSC with Pt sputtered StS 316 as a counter electrode before and after the light soaking test measured by EIS in the dark. Note that $R_{CT} = R_{PE}$ and $CPE_{CT} = C_{PE}$. Figure is from Publication V.

3.3. Raman spectroscopy

Raman spectroscopy is a spectroscopic technique that relies on inelastic scattering (the frequency of photons changes after interaction with the sample), also known as Raman scattering, of a monochromatic light usually from a laser source. Upon interaction with the sample, the photons of the laser get absorbed by the sample and then reemitted by it. If the frequency of the reemitted photons is the same as the original frequency of the incident photons, it is Rayleigh scattering. If the frequency of these

reemitted photons either shifted up (anti-stokes) or shifted down (stokes) from the initial frequency value, it is called Raman scattering. In confocal microscopy, it is possible to focus on a small area undisturbed from the signals originating from unintended area with the help of confocal optics. Thus Raman allows the analysis volume to be as small as a few cubic micrometers. Mostly, Raman spectroscopy is used for qualitative purposes, e.g. determination of molecular structures, but also quantitative analysis has been reported [38,39]. The intensity of a Raman peak $I(\nu)$ is given by [38]:

$$I(\nu) = I_0 K(\nu) C \quad (6)$$

where I_0 is the intensity of the incident laser beam, $K(\nu)$ includes the frequency dependent terms, ν is the Raman shift in cm^{-1}, and C is the concentration of the measured specie. By assuming that the intensity of the laser power and the frequency dependent factors remain constant, the intensity of species peak at a particular Raman shift becomes directly proportional to its concentration. Therefore, the height of the Raman peak can be used to estimate the concentration of different species [38].

In this work, the Raman spectroscopy was performed by using a HORIBA Jobin Yvon LabRam 300 micro-Raman spectrometer. It was equipped with a 514 nm argon laser. The power of the laser beam was 1.24 mW which was further reduced to 0.0124 mW by using a filter in the measurement setup. In the measurements, the laser spot size was approximately 5000 μm^2 and the measurement time was 5 seconds for a single measurements.

The main advantages of the Raman spectroscopy are that it is a fast and non-destructive technique (i.e. does not require cell disassembly) giving chemical information which may help to understand the degradation mechanisms occurring in DSCs. However, there is a limitation to this technique with regards to the application in DSCs that too intense beams of laser with longer exposure time may destroy the DSC components, in particular the dye. Another important issue is that the very high intensity of the laser beam focused on a small area on PE may corrupt the data by temporarily or permanently changing the dye structure. In this work, the aim was to avoid any damage to the cell components without compromising

on the quality of the data. Therefore, an optimum beam intensity and measurement time was used that gave good quality data and the cell remains undamaged. However, there is still a possibility that exposing the dye to the laser beam might change the time for which a dye stay in oxidized state which is more vulnerable to degradation (substitution of SCN^- ligand with electrolyte additives) as compared to dye in ground state. This raises a concern that the measured Raman spectra of SCN^- might be partly or fully affected by the intense laser beam. However, in this study (Publication VII) Raman spectroscopy is applied to study the effect of spatial distribution of electrolyte components, fortunately different rate of regeneration of dye would still serve the purpose of studying the spatial variation. A typical Raman spectrum obtained from the PE of a DSC measured is shown the Figure 8.

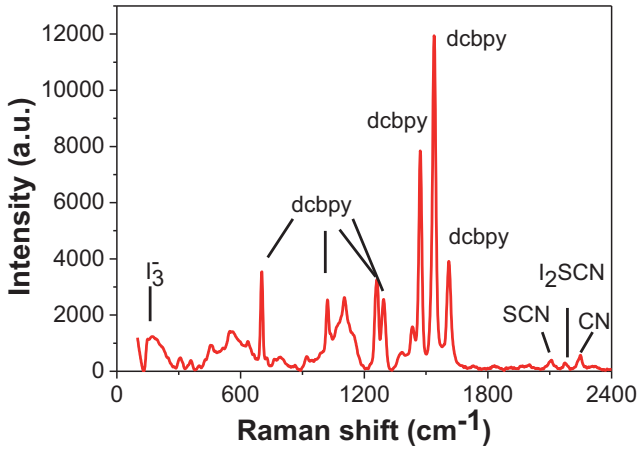

Figure 8. Typical spectrum obtained from the PE of a DSC using 514 nm laser beam

In order to find the photon flux falling on the spot used for the measurement, we can calculate the photon flux using Eq. 7 as follows:

$$\emptyset\ 514nm\ = \frac{P}{E_{photon}A}\left[\frac{1}{m^2 s}\right] \qquad (7)$$

Where P is the power of the incident laser beam, E_{photon} is the energy of a single photon of wavelength 514 nm and A is the area of the spot where the

laser beam was focused on the sample. The energy of a single photon can be calculated using Eq. 8.

$$E_{photon} = \frac{hc}{\lambda}[J] \qquad (8)$$

The short circuit current density generated by the laser beam is given by Eq. 9.

$$i_{SC}^{Raman} = q_e\, \eta_{IPCE}\, \emptyset\ 514nm\ [\frac{A}{m^2}] \quad (9)$$

Where q_e is the elementary charge and η_{IPCE} is the quantum efficiency of DSC at 514 nm wavelength (here approximately 55%). The ratio of the short circuit current density generated by the laser beam to the one generated under 1 Sun light intensity gives the light intensity of the laser beam used in the measurement in terms of unit Sun. The laser beam intensity used in this work is calculated to be approximately 4 Sun.

3.4. Segmented cell method

The understanding of the degradation mechanisms is vital to improve the overall stability of the cells. In this regard a method called 'segmented cell method' is useful as it may be used to isolate or separate different kind degradation processes. A segmented cell consists of two or more segments electrically isolated from each other. In a segmented cell two or more cells share the same electrolyte. The idea is that any degradation in one segment related to the electrolyte may be seen in other cells as shown in Publication I and elsewhere in the literature [40]. The segmented cell method can also be used to investigate variation in performance due to spatial distribution of electrolyte as in Publication VII. A schematic of the different possible configurations that may be applied in a segmented cell is shown in Figure 9.

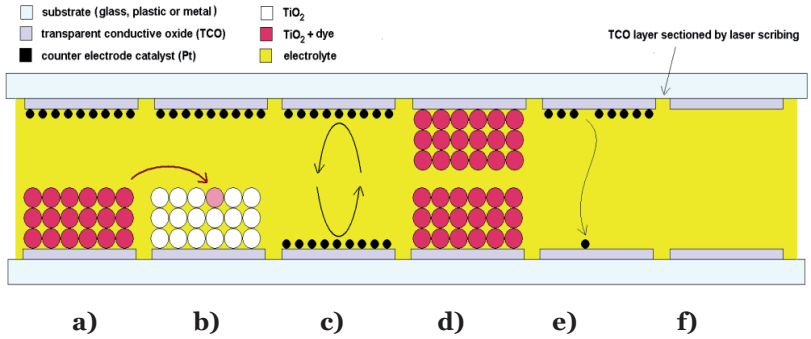

Figure 9. Segmented cell with different segment configurations: a) PE-CE, b) dye free PE-CE, c) CE-CE, d) PE-PE, e) CE-TCO, f) TCO-TCO. (PE = photoelectrode, CE = counter electrode, TCO = transparent conducting oxide). Figure from Publication I.

Depending on the degradation mechanism under study, the segmented cell can be applied in suitable configurations to effectively analyze the degradation. For instance, a three segmented cell (dye free-PE-CE, PE-CE, TCO-TCO) can be used to study the dye desorption phenomenon. Any dye desorbed from the PE-CE segment may sensitize the photoelectrode at the dye free PE-CE segment via the electrolyte which can be seen as a dramatic improvement in the performance. Finally the TCO-TCO segment can be used for the optical measurements to analyze the chemical composition of the electrolyte. It also provides the possibility to study the TCO-electrolyte interface. A chemical analysis of the electrolyte can be performed using optical techniques together with electrical analysis. The results would be useful to understand the cause and effect of the dye desorption. Similarly, the stability of the electrolyte and CE can studied by using three segmented cell (PE-CE, CE-CE, TCO-CE). For instance, as the charge transfer at the TCO is very poor, if any detached catalyst particle from the CE reaches the TCO it would dramatically improve the electrochemical properties of the TCO.

A huge advantage with the segmented cell method is that it allows to apply various in-situ analysis techniques. The Figure 10 shows a range of possible measurement techniques that can be used in-situ (I-V measurements, EIS, IPCE, Raman spectroscopy, FTIR spectroscopy, NIR spectroscopy, UV-Vis spectroscopy) or ex-situ (SEM, EDX) in parallel.

There are few limitations to this method i.e. the response time depends on the diffusion through the electrolyte and it may be non-quantitative.

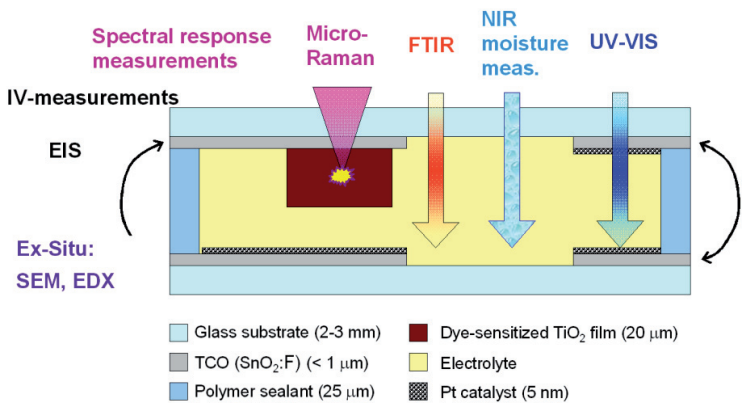

Figure 10. Analysis on segmented cell using various in-situ and ex-situ techniques. Figure by courtesy of Janne Halme.

3.5. Image processing method

As the appearance of the main components may change upon degradation, quantitative visual analysis can be a fast and easy way to investigate stability. In this regard, here a new in-situ method using image processing technique is introduced. Image processing has already been successfully implemented in many applications such as automation and robotics, sorting of goods in many industries, and city traffic control. A similar monitoring technique has been reported to study the sensitization of photoelectrode using gray-scale format [41]. In this work to study the degradation related to the electrolyte (Publication III), true color format i.e. Red, Green, Blue (RGB) is used since color information is essential to differentiate the degradation process. Whereas, to study the dye sensitization process (Publication IV), gray-scale format is used since in this case the intensity of color of the dye sensitized TiO_2 film is important. In both cases proper color calibration was performed to get high quality quantitative results.

3.5.1. Measurement setup and procedure

The measurement setup used in the image processing method consists of a color sensitive camera, a set of LEDs mounted on a movable tray and a platform on which cells can be placed with white background as shown in the Figure 11. The camera (Olympus E-620) selected for this system features an image resolution of 12.3 Megapixels and a high speed live MOS sensor of size 17.3 mm (Horizontal) x 13.0 mm (Vertical). The setup is isolated from the external light by covering it from all sides with a black out canvas. The cells are mounted on a portable platform with the help of the current collectors which makes it possible to measure them electrically as well. In order to take photographs from the same distance and position with respect to the samples, the portable platform is placed to a fixed position under the movable tray. The movable tray can be then moved so that it is possible to take photographs of all the cells from the top separately. This way the lighting conditions and position of the camera with respect to each cell remain the same allowing the comparison of the photographs possible with least noise. The photographs are taken in RAW format, which is also referred as digital negative, to extract maximum information from the images.

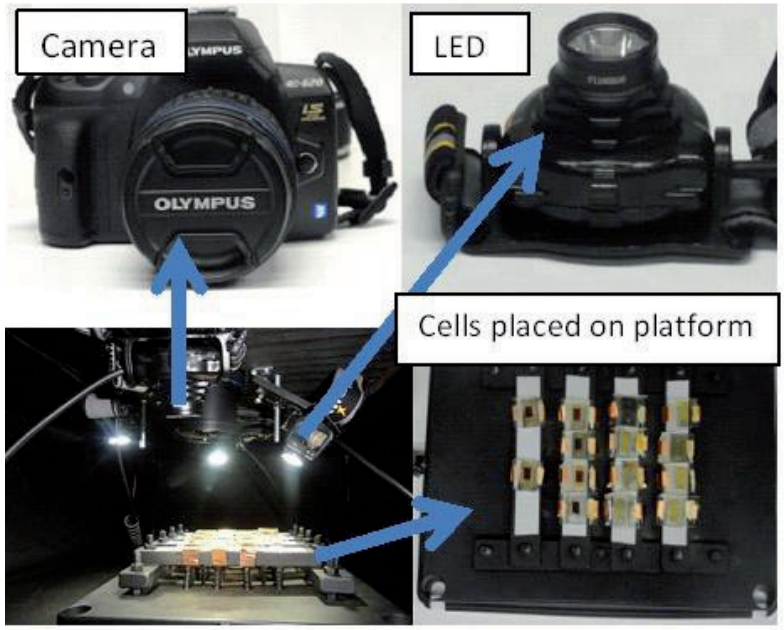

Figure 11. The measurement setup used in the image processing method consisting of a color sensitive camera (Olympus E-620) and a set of four LEDs mounted on a movable tray. The cells are placed on a fixed platform underneath the movable tray. Figure from Publication III.

Before taking the photographs of the actual cells, the lighting conditions need to be balanced with a so called 'color checker passport' to avoid any light noise. This is a critical step for getting proper quantitative color information from the images. The color checker passport consists of a grey and a colored part. A photograph of the grey plate of the color checker passport is taken at the same lighting conditions as the DSCs would have. It creates a profile which is applied to the camera settings. Next, it is important to make sure that the color shades are the same for all photos of DSCs taken at different times. For this purpose, a photo of the color palette of the color checker passport is taken with the same camera settings and lighting conditions. The image is used to generate a color profile in Lightroom 3 software. Later all the photographs are taken using the same camera settings. If the images are taken in conditions in which the lighting

cannot be easily controlled such as outdoors, every image should have its own color calibration. This could be done by doing separate white balancing using the grey part of the color checker passport before each photograph and placing the color part of the checker passport next to the studied cell for each image. In such case it is important to make sure that the lighting is homogenous across the cell and the color checker. For this reason for instance the use of flash is not advisable in particular in close up images as it tends to result in very uneven illumination across the image.

3.5.2. Analysis

In the analysis, the first step is to generate a color profile that takes into account of any variation of the back ground lighting conditions and to make the comparison of the color possible. For this purpose, the photograph of the color checker passport in RAW format is used. The Lightroom 3 software reads the RAW format photograph of the color checker passport and generates a color profile which is then applied on all the photographs of DSCs in RAW format. After the application of the generated color profile, the modified photographs in RAW format are converted to JPEG format using the same Lightroom 3 software. Once the conversion to JPEG format is done, the images are ready for further processing. Finally, Matlab software is used to import and process the JPEG images to evaluate the RGB (red, green, blue) values for each of the image. In a 24-bit data format of the JPEG image, the data is presented in the form of RGB (red, green and blue) model which is also known as a true color model. In this model, each pixel in the image is composed of three separate 8-bit values corresponding to red, green and blue (RGB) component respectively. In an 8-bit format, each red, green and blue values span from 0 (binary 00000000) to 255 (binary 11111111). Typical RGB values of different colors in 8-bit data format are given in the Table 1.

Table 1. RGB values for 8-bit data format (0 and 255 corresponds to binary 00000000 and 11111111 respectively). Table from Publication III.

Color	Red	Green	Blue
Red	255	0	0
Green	0	255	0
Blue	0	0	255
Yellow	255	255	0
White	255	255	255
Black	0	0	0

3.5.3. Correlation between electrolyte concentration and color

In order to study the degradation of electrolyte which is often due to decrease in the tri-iodide concentration in electrolyte (i.e. bleaching of the electrolyte), a relationship between the tri-iodide concentration in the electrolyte and the corresponding RGB pixel values obtained from their appearance needs to be established. For this purpose, DSCs prepared from a series of electrolytes with different concentrations of iodine were processed using image process method as explained in Sections 3.5.1 and 3.5.2. Iodine is the main source of tri-iodide in the electrolyte. The RGB data of cells with varying concentration of iodine are shown in Figure 12. It shows that with increasing the concentration of iodine, which is the source of tri-iodide in the electrolyte, the blue pixel values are decreasing while the red and green pixel values stay practically constant. Within the range from 0.025 to 0.1 mol/dm^3 of iodine in the electrolyte, the resolution of image processing method is calculated to be 7.35×10^{-4} mol/dm^3 per one blue pixel value. This means that one unit change in blue pixel value corresponds to

1.47% changes in the tri-iodide concentration of a standard electrolyte (0.05M I_2) for DSC.

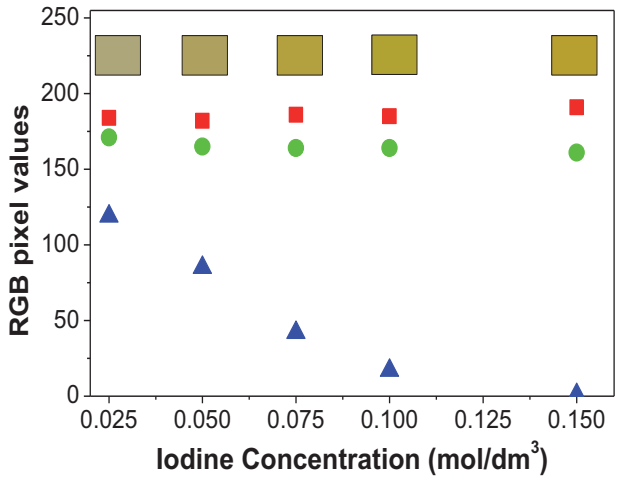

Figure 12. Image processing in terms of RGB pixel values for a series of electrolyte containing varying concentration of iodine. (Red = R, Green = G, Blue = B). Figure from Publication III.

4. Results and Discussion

This chapter is divided into four sections. The first section presents the state of the art of the DSC's stability and covers the general degradation mechanisms in the DSCs. In the second section, a new method based on image processing is demonstrated to study the performance and stability of the DSCs. In third section, stability of the flexible metal substrates is discussed. Finally in the fourth section, segmented cell method is used to study the performance degradation in the DSCs due to spatial distribution of electrolyte components.

4.1. Degradation mechanisms in the DSCs (Publication I & II)

This research work was started with a literature review (Publication I) to find out the current knowledge regarding the stability of DSCs. The idea was to critically investigate the literature to find out the key issues affecting the lifetime of a DSC.

As a DSC consists of several different materials, their internal chemistry and their interaction with other materials play a key role in the stability of the DSC. In addition, the stress factors such as temperature, light and humidity can affect the stability of the DSC by accelerating the existing degradation mechanisms or by generating new degradation processes. For many of these mechanisms various explanations have been presented.

It was found that although there were several studies done on the stability of the DSC, there was a lack of systematic studies which separates the hypothesis and mere speculations from solid experimental evidence regarding the cause and the mechanisms of degradation. With this motivation, in Publication I several hypotheses were studied critically covering the degradation processes at the photoelectrode, at the counter

electrode and in the electrolyte under different conditions (temperature, light intensity and moisture).

4.1.1. Stability tests for DSCs

The basic aim of an accelerated ageing test is to estimate the lifetime of a solar cell in a relatively short period of time. The solar cells are stressed under certain conditions where the degradation mechanisms get accelerated. A thorough experimental data makes it possible to establish a standard test for a specific solar cell type. So far no standards have been established for the stability testing of DSCs. Accelerated ageing tests that are used for thin films defined in standards referred as ASTM E, IEC 61646, IEC 61215 and JIS C-8938 are currently being used for DSC. However, it is important to note that the degradation mechanisms in DSC are different from thin film solar cells and thus these tests may not be fully applicable. Therefore, it is important to establish standard tests for DSCs to estimate their lifetime. It is also important to keep the final application in mind while defining the standard tests. For instance, indoor applications such as toys are usually exposed to only mild and quite constant temperatures while solar panels placed outdoors are subject to weathering.

It is also important to define how much decrease or increase in performance of a DSC can be considered stable for certain duration of time. In DSC literature, generally when the variation in performance is within 10% [21,22,23], the DSC is considered to be stable. However, in standards for thin films solar cells, only 2% change in performance is allowed to be declared stable. At the same time, it is important to set the criteria to evaluate the performance of a DSC i.e. whether η alone should be monitored or all performance parameters including i_{SC}, V_{OC} and FF should be examined. As discussed in the Publication I, at the moment, light soaking test at room temperature (RT), 60°C and 80°C, and thermal test at RT, 60°C and 80°C are the most commonly used tests to investigate the stability of a DSC [21-23].

4.1.2. Degradation at the photoelectrode

The instability of the photoelectrode can be regarded as a major reason for the instability of a DSC. Any degradation in the photoelectrode can greatly affect the performance of a DSC specially the i_{SC}. Generally, the degradation at the photoelectrode can be categorized into dye desorption, dye degradation and degradation in the electron collection.

The dye desorption has been presented in several articles as a reason for the degradation in i_{SC} of a DSC when stressed at 85°C in dark conditions [42,43]. It has also been regarded as the main reason for the failure to pass 80°C thermal test. There are several speculations given in the literature to explain the degradation due to dye desorption. One speculation explained the dye desorption as a reason of shift in the equilibrium between the dye desorped onto the TiO_2 and the dye dissolved in the electrolyte due to change in temperature [43]. At high temperature i.e. 80°C, the equilibrium shifts in the favor of dye desorption into the electrolyte resulting in a lower performance of the DSC. On the other hand, at lower temperature i.e. 45°C under illumination the equilibrium shifts in the favor of dye re-adsorption onto the TiO_2 film leading to the recovery of the DSC performance. However, this hypothesis is lacking direct solid evidence other than that deducted from the changes in the photovoltaic parameters. Another speculation about dye desorption states that the decomposition products in the electrolyte co-adsorb onto the TiO_2 surface favoring desorption of dye at high temperature [44]. It has also been suggested that as TiO_2 is hydrophilic in nature and even a small quantity of water in the DSC may lead to desorption of dye [45]. This speculation is supported by the fact that only hydrophobic dyes such as Z907, K77 and K19 have been reported to pass 80°C thermal test for 1000 hours [22,46,47,48].

Both N719 and Z907 dyes have been suggested to get degraded at elevated temperatures i.e. higher than 80°C as a result of thiocyanate ligand (SCN) exchange with the electrolyte solvent MPN or the additives in the electrolyte such as 4-tert butyl pyridine (TBP) [49,50]. The SCN ligand substitution reaction with TBP is shown in the Figure 13. The worst case scenario would be that in all the dye molecules one of the SCN ligands gets exchanged with TBP in the electrolyte (i.e. 100% degraded dye). In order to examine this, in

Publication II a comparative study was performed between the fresh N719 dye and a synthesized dye in which one of the SCN ligand is replaced with TBP (N719-TBP) to mimic the worst case scenario.

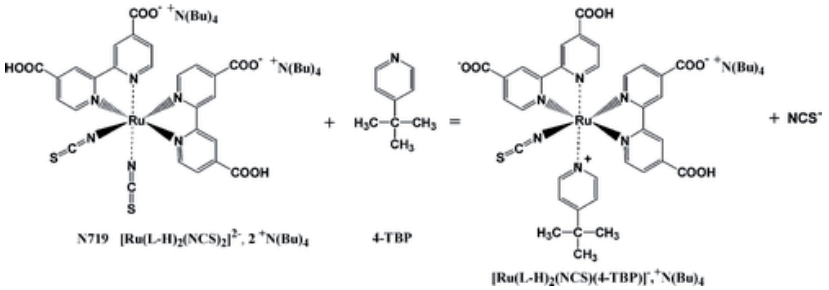

Figure 13. Degradation of the N719 dye by substituting one of the SCN ligand with TBP. Figure from Publication II.

Interestingly, the DSCs with N719-TBP showed 50% lower efficiency compared to DSCs using N719 as a sensitizer as shown in Figure 14 and Table 2. The comparative analysis of N719 dye and N719-TBP dye based DSCs revealed that the reduction in the performance in the case of N719-TBP based DSCs is caused by a lower light harvesting efficiency due to approximately 30 nm blue shift in the absorption spectrum, a decrease in electron diffusion length around 50% due to a lower electron recombination resistance and an approximately 14% decrease in the charge separation efficiency as compared to the N719 dye.

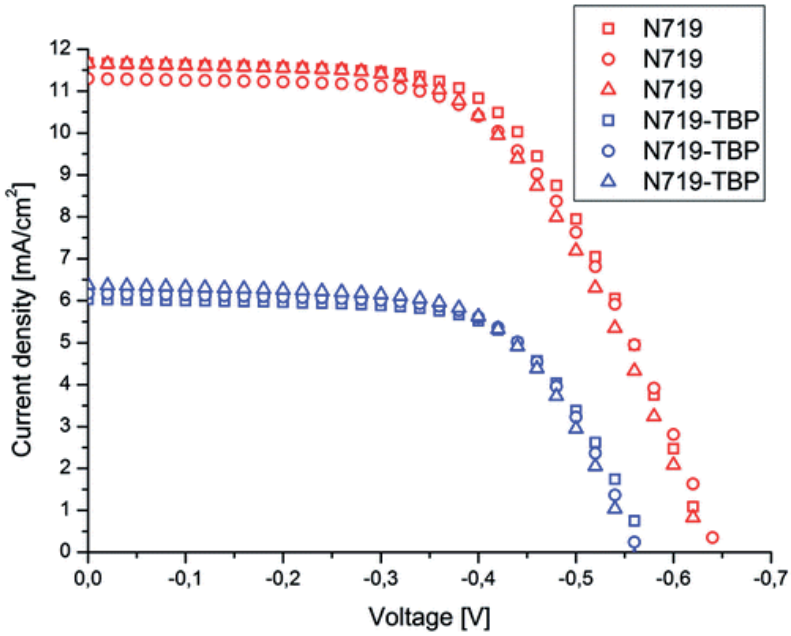

Figure 14. The I-V curves of the N719 and the N719-TBP based DSCs measured under 1 Sun light intensity. Figure from Publication II.

Table 2. The performance parameters of the N719 and N719-TBP based DSCs. Data from Publication II.

Dye	i_{SC} (mA/cm²)	V_{OC} (V)	*FF* (%)	η (%)
N719	11.7±0.2	-0.65	57.3±1.3	4.3±0.1
N719-TBP	6.3.3±0.1	-0.57±0.01	63.3±0.3	2.2

As mentioned earlier there are in general a series of other mechanisms that affect the stability of the PE that are not related to the dye: Firstly, the degradation in the TiO_2 film may cause an increase in the electron transport resistance in the TiO_2 film or the contact resistance of the film. Secondly, side products formed in the electrolyte and/or detachment of catalyst

particles at the CE that would diffuse and attach to the PE can also affect the stability of the PE. Such changes could then also lead to a decrease in the electron life time and the recombination resistance. The decreased electron lifetime and increased recombination are known to affect the performance characteristics of the DSC especially V_{OC}. The application of insulation layers such as Al_2O_3 [51,52] or MgO [52,53] onto the PE has been reported to reduce the recombination from the TiO_2 film to the electrolyte. This kind of blocking layers might also improve the stability of the PE by hindering the harmful contamination.

Moreover, the quality of the TiO_2 film plays an important role in the stability of PE. It is evident from the fact that when DSCs are made on rigid glass based substrates where it is possible to sinter the TiO_2 film at 450°C, there is larger variety of printable inks or pastes to be used at the PE. However, in case of plastic based DSCs where the temperature treatment is restricted to 150°C, there is lesser variety of high quality printable inks or paste.

4.1.3. Degradation at the counter electrode

As the CE is composed of a catalyst layer deposited on a substrate, any degradation to the catalyst layer or substrate would have detrimental effects on the performance and stability of DSC. The performance of CE is determined by its catalytic activity i.e. charge transfer resistance at the counter electrode (R_{CE}) which is usually measured through EIS.

Factors that may affect the catalytic performance at the CE may be divided into two categories caused by physical and chemical changes. Physical effects include the detachment of the catalyst particles and poor adhesion on the substrates. Furthermore, in the case of plastic substrates, the permeability to water and oxygen may also adversely affect the stability of DSC. The physical stability depends on the type of the substrate, the catalyst material and the deposition method. For instance thermally platinized glass based DSC are highly stable even at high temperature i.e. 80°C [22,46,47,48], whereas sputtered Pt based DSC degrade in couple of days [54] at 80°C. Carbon based DSCs have demonstrated good stability at RT [55], however, no stability results are reported at 80°C. Carbon

nanotubes (CNT) films deposited on ITO-PET showed lower stability even at RT [56,57]. In addition, deposition of by-products in the electrolyte onto the CE may also affect the catalytic performance of the CE. Conventional tape tests such as ASTM 3359 and bending tests have been used to test the adherence of the catalyst particle film on the substrate [58].

Chemical effects include detrimental chemical reactions between the catalyst particles or substrate with the electrolyte. The chemical stability depends also on the type of the substrate, catalyst material, the deposition method as well as the corrosiveness of the electrolyte. Techniques giving chemical information such as optical infrared spectroscopy may be useful to examine the by-products in the case of any degradation at the counter electrode. Any decrease in the catalytic activity can be studied using EIS. Furthermore, in the case of corrosion to the substrate or catalyst film, SEM together with EDS or EELS give information about the degrading chemical reaction as shown in Publication V.

4.1.4. Degradation of the electrolyte

Most of the electrolytes for DSCs are based on iodide/tri-iodide redox couple. These kinds of electrolytes have a yellow color due to the presence of tri-iodide. The tri-iodide plays a critical role in the cell by transferring the charge from the PE to the CE by means of diffusion. Any degradation to the electrolyte causing decrease in the tri-iodide concentration might thus lead to the degradation of the DSC. The stability of electrolyte in a DSC depends on several factors such as the type of the CE, the coverage of the dye onto the TiO_2 and the influence of external factors such as humidity, UV and visible light, and temperature.

The electrolyte in the DSC was shown to be very stable at light soaking at RT when using thermally platinized or sputtered FTO glass as CE in Publication V. It shows that light soaking alone is not harmful for the electrolyte. In another study no bleaching of electrolyte was observed at 85°C when using thermally platinized CE. The same study revealed that bleaching of the electrolyte occurred when DSCs were exposed to light soaking at 85°C. Interestingly, the degraded DSCs at 85°C recovered their

performance when brought to RT [59]. It seems that some reversible reactions occur under that conditions and as the temperature went down, the equilibrium was shifted to the other side. It shows that light soaking at high temperatures is very challenging for the stability of the DSC.

The degradation in the concentration of tri-iodide can be easily studied by measuring changes in the limiting current density (i_{lim}) as done in Publication III. In the extreme case, loss of triiodide can even limit the i_{SC} by the decrease in the limiting current density. The changes in the triiodide concentration can alternatively be studied with EIS as an increase in the Nernst diffusion impedance of tri-iodide. Indeed, the degradation in the electrolyte which causes increase in the diffusion impedance results also in decreasing the *FF*. The chemical analysis of electrolyte using optical (Publication VII) and spectroscopic techniques such as Raman spectroscopy and IR spectroscopy may be very useful to find the cause of the degradation and the by-products formed. As the degradation involves the change in the color of the electrolyte, image processing method can be utilized to study the bleaching of the electrolyte as in Publication III.

4.1.5. Sealing issues

One of the most challenging factors that can affect the stability of a DSC is the sealing of the device. The failure of the sealing may result in either a gradual loss in the performance or sudden death of the cell. Firstly, the liquid electrolyte can leak out of the cell. Secondly, a poor sealing may not withstand the high vapor pressure of the solvent and other additives at high temperature i.e. 80°C and result in a failure. Thirdly, impurities such as oxygen and water may also penetrate into the DSC and harm the device. Especially in the case of the plastic substrates, which are permeable to oxygen and water, sealing becomes an even more challenging issue. In addition, the sealing should also protect the current collectors from the corrosive electrolyte.

The sealing should be mechanically, chemically and thermally stable for the working conditions to which the DSC is expected to be exposed. From a mechanical point of view, it should withstand external factors such as rain and even hail storms and internal factors such as gas bubbles and high

vapor pressure of the solvent inside the DSC. From a chemical point of view, it should be stable with electrolyte and with the other components of the DSC. From a thermal point of view, it should be flexible enough to withstand any thermal expansion of the electrolyte but it should also remain stable as sealant.

A polymer based hot melt foil Surlyn 1702 is the most common sealant used in DSCs and also chemically stable with electrolyte. However, this sealant has low softening temperature i.e. below 80°C which results in poor stability at high temperatures i.e. 80°C. Another polymer based hot melt foil Bynel has been shown to be an excellent sealant for DSCs which work properly even at high temperature as the softening temperature is above 80°C [48]. Another sealing method based on glass frit which is commonly used in plasma display panel has also been applied to DSC. It also shows excellent stability at high temperatures e.g. 80°C [60]. However, there are a few limitations due to the fact that glass frit sealing requires a high processing temperature i.e. around 600°C [42,60,61] in particular the electrolyte and the dye need to be introduced in the cell after the high temperature sealing step.

4.1.6. Cross-line between performance and stability limiting factors

The performance parameters, i.e. i_{SC}, V_{OC} and *FF*, are limited and affected by different processes in the DSCs. For instance i_{SC} is usually limited by the absorption and injection by the dye. That is why any decrease in i_{SC} is usually ascribed to the degradation of the dye. However, it is not always true as mentioned earlier for instance decrease in the iodine concentration might limit i_{SC}.

There are often several degradation mechanisms occurring in the DSC simultaneously. It may happen that a particular degradation becomes dominant and limit the performance parameters of the cell. For instance, under severe conditions when the i_{SC} is limited by the i_{lim} instead of the dye due to the decrease in the tri-iodide concentration in the electrolyte, i_{SC} is no more sensitive to the degradation of the dye. Therefore, before making

any conclusion about the stability of a certain component in the DSC, it is important to keep in mind while doing the analysis that which process is limiting a particular performance parameter.

4.1.7. Current state of the art of stability of DSC

The stability of the DSCs depends on the stability of individual components as well their combination in the cell, in particular the dye-electrolyte combination. The state of the art of stability for important dyes that have been used in DSCs is presented in the Table 3. Generally, hydrophilic dyes such as N3, N749 and N719 are not stable for 1000 hours under 80°C. However, the amphiphilic dyes such as Z907, K19 and K77 have been reported to be stable for 1000 hours.

Table 3: List of important dyes with their molar extinction coefficients and their stability status at 80 °C. Data from Publication I.

Dye	Peak molar extinction coefficient (M^{-1} cm^{-1})	Stability at 80 °C for 1000 h
N749	7.8×10^3 [62]	Unstable [66]
N719	14×10^3 [63]	Unstable [46,64]
Z907	12.2×10^3 [64]	Stable [46]
K19	18.2×10^3 [64]	Stable [64,48]
K77	19.4×10^3 [65]	Stable [22,65]
C103	18.8×10^3 [23]	Not known
C104	20.5×10^3 [66]	Not known
TH304	41×10^3 [67]	Not known

The state of the art of stability for important types of electrolyte that have been used in DSCs is presented in the Table 4. Generally, all the three types of electrolyte i.e. liquid electrolyte, polymer gel electrolyte and ionic liquid based electrolyte have been shown to be stable for 1000 hours under 80°C. However, it is important to mention that this high stability is achieved only when using amphiphilic dyes. The stability data in the Table 4 is presented according to the maximum efficiencies achieved for the respective electrolyte.

Table 4: The state of the art of DSCs using different kinds of electrolytes with respect to their stability at two challenging conditions. Data from Publication I.

Electrolyte type	Dye	Light soaking at 60 °C for 1000h	Thermal stress at 80 °C for 1000 h	Efficiency (%)
Liquid electrolyte	C103 [23] K77 [22]	Passed Passed	- Passed	9.6 9
Polymer gel electrolyte	Z907 [46]	Passed (55 °C)	Passed	6
Ionic liquid electrolyte	C103 [23] K77 [22] Z907Na [21]	Passed Passed Passed	- Passed -	8.5 7.6 8.2

4.2. Visual analysis of DSC (Publication III & IV)

The most important components of a DSC i.e. dye, electrolyte and catalyst material have specific colors. For instance, the N719 dye which is the most commonly used dye in DSC has a red color, the electrolyte has usually a yellowish color due to the presence of tri-iodide in the electrolyte whereas Pt catalyst particles have a grayish color. The degradation of these components may cause visual change in the appearance of the cell. For instance, the desorption of the dye into the electrolyte that has been proposed to occur in literature [42,43] at elevated temperature i.e. 80°C would change the color of the electrolyte towards reddish color. Similarly, a decrease in the tri-iodide concentration in the electrolyte could cause a bleaching of the electrolyte [68,69]. Any degradation reaction involving the tri-iodide and the catalyst material would lead to the bleaching of the electrolyte and consumption of the catalyst particles [70,71]. In the case of a leakage of the electrolyte through the sealant, the marks of the leaked electrolyte can be seen visually. In the worst case, the leaked electrolyte may corrode the silver grids which can also be seen visually [72]. It shows that there is some relationship between the performance of DSC and its appearance. In this work, visual analysis is done using image processing method described in section 3.5 to demonstrate the applicability of the method to study the bleaching of electrolyte and the effect of sensitization time on DSC performance.

4.2.1. Bleaching of electrolyte

The bleaching of the electrolyte has been reported in the literature and it has been to some extent been already covered in Section 4.1.4. In Publication III, three different configurations of cells were made i.e. PE-CE, CE-CE and TiO_2-CE as shown in the Figure 15 to isolate the degradation processes. As the purpose of this work is to demonstrate the image processing method to investigate the stability and performance of a DSC, all the cells were exposed to extreme conditions i.e. UV+Vis illumination at 85°C to accelerate the bleaching process. In addition to the image processing method, I-V measurements in dark and under 1 Sun at room temperature were also performed on day 0, 1, 5 and 10 respectively. The purpose was to correlate the visual changes with the changes in the electrical performance. After the ageing period of 10 days, the cells were exposed to multiple cyclic

voltammetry scans between -1.5V to 1.5V in order to see whether the bleached electrolyte recovers its color as observed by Hauch et al. [26] or not.

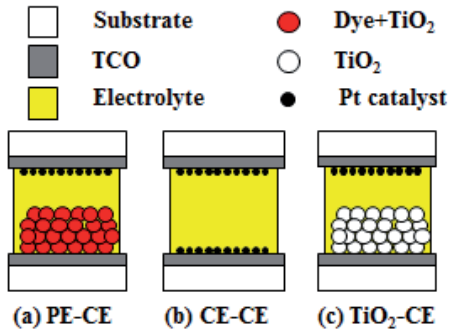

Figure 15. Three different cell configurations (a) PE-CE, (b) CE-CE, and (c) TiO_2-CE employed to isolate the degradation mechanisms (PE = photoelectrode, CE = counterelectrode, TCO = transparent conducting oxide). Figure from Publication III.

As discussed in Section 3.5, the bleaching of the electrolyte would result in increasing blue pixel value. Interestingly, the bleaching trend was different in different configurations as shown in the

Figure **16**. The normal DSC, referred here as a PE-CE cell, showed a gradual increase in the blue pixel value representing a gradual loss of yellow color of the electrolyte. The CE-CE cell did not show much change in the blue pixel value representing no change in the electrolyte color. Hence, it can be concluded that the CE (thermally platinized on FTO glass) and electrolyte themselves are very stable under the ageing conditions and bleaching involves the PE. The TiO_2-CE cell showed sharper rise in the blue pixel value as compared to the PE-CE cell indicating a more rapid bleaching in the case of the TiO_2–CE cell. As the PE is comprised of TiO_2 porous film sensitized with photosensitive dye, the different bleaching rate of the PE-CE cells and the TiO_2-CE cells shows that in fact the TiO_2 film is responsible for the bleaching of the electrolyte. Moreover, it can be deducted that the dye on the TiO_2 film is actually protecting against the bleaching reaction. Interestingly, in all the three cases electrolyte recovered its color to some extent as shown by the decrease in the blue pixel value when the cells were

exposed to multiple cyclic voltammetry scans between 1.5V and 1.5V after the ageing period.

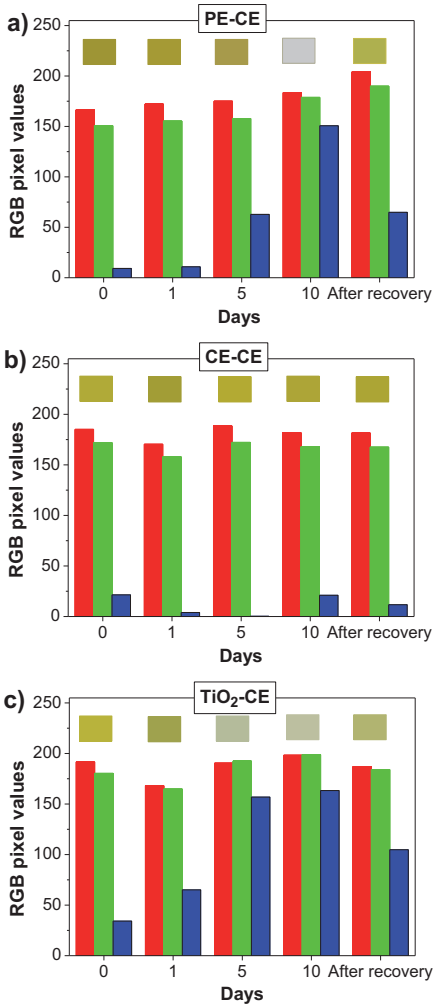

Figure 16. The RGB pixel values of images in 8-bit format as a function of time for different cell configurations: a) PE-CE, b) CE-CE, c) TiO_2-CE aged under UV+Visible light at 85°C for 10 days followed by cyclic I-V measurements to recover the electrolyte color after 10 days . (Binary 00000000 and 11111111 corresponds to decimal 0 and 255 respectively). Figure from Publication III.

I-V measurements were performed in dark to see the effect of decreased tri-iodide concentration on i_{lim}. i_{lim} is directly proportional to the equilibrium concentration of tri-iodide $c_{I_3^-,0}$ in the case where tri-iodide is the only current limiting ion [26]:

$$i_{lim} = \frac{4FD_{I_3^-}c_{I_3^-,0}}{d}, \tag{10}$$

where, F is the Faraday's constant, $D_{I_3^-}$ is the diffusion coefficient of tri-iodide, and d is the thickness of the electrolyte layer. i_{lim} can be seen as the saturation current density of a reverse biased cell.

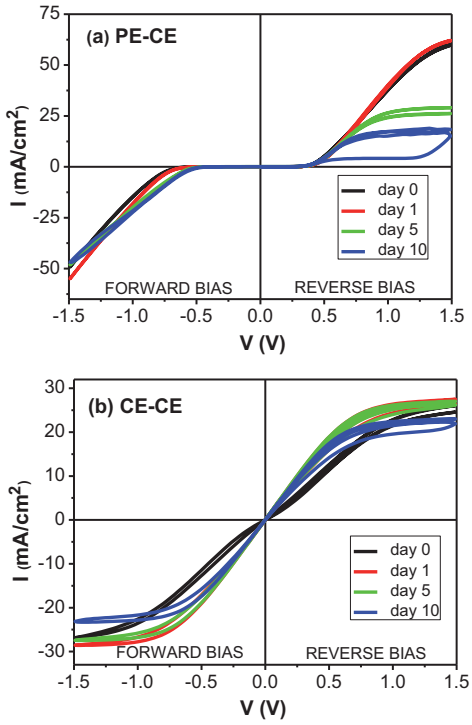

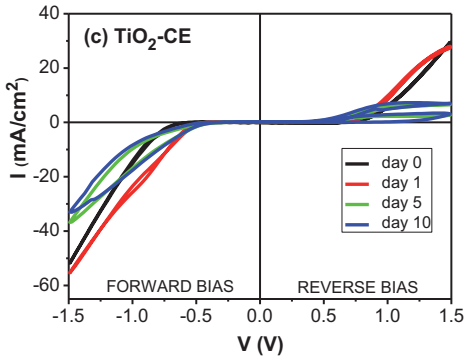

Figure 17. I-V curves of cells with different configurations in the dark: a) PE-CE, b) CE-CE, c) TiO_2-CE. Figure from Publication III.

Figure 17 shows I-V curves of the PE-CE, CE-CE and TiO_2-CE cells over a voltage range of -1.5V to 1.5V measured in dark. i_{lim} of the PE-CE cells decreased gradually as shown in Figure 17a as expected from the gradual increase in the blue pixel value (representing gradual decrease in the tri-iodide concentration leading to gradual bleaching of the electrolyte) shown in

Figure **16**a. i_{lim} was indeed so low on day 10 that it was limiting the i_{SC}. However, prior to day 10 i_{lim} was much higher (above 25 mA/cm²) compared to i_{SC} (max 11 mA/cm²) which means that i_{SC} was not limited by decreased i_{lim}. In the TiO_2-CE cell, the i_{lim} decreased sharply from a value of more than 29 mA/cm² to 0.02 mA/cm² during the ageing period in accordance with the faster rate of increase in the blue pixel value shown in

Figure **16**c. This represents a faster decrease in the tri-iodide concentration in the TiO_2-CE cell leading to the faster bleaching of the electrolyte as compared to the PE-CE cell. Interestingly in the CE-CE cell the i_{lim} stayed roughly the same as expected based on the image processing results shown in

Figure **16**b where the blue pixel values remained practically constant. This represents no significant change in the tri-iodide concentration leading to no significant bleaching of the electrolyte. Hence, the results obtained using I-V curves measured in dark are in agreement with results obtained using image processing method.

4.2.2. Effect of dye sensitization time on performance

The sensitization of the dye on the TiO_2 plays the most important role in the operation of a DSC. The performance of a DSC is greatly affected by the dye sensitization time. For instance, if the dye sensitization time is too short than the amount of dye chemisorbed onto the TiO_2 is too low. Similarly if the sensitization time is too long then the dye starts getting physiosorbed onto the monolayer of dye already absorbed on the TiO_2 particles. In both cases, the performance of the DSC is adversely affected. Hence, there is a need to optimize the dye loading time and conditions i.e. optimum temperature. In Publication IV image processing method was used to study the effect of dye sensitization time onto the TiO_2 film. The main aim of this study is to demonstrate the applicability of image processing method to monitor the dye loading process and its effect on the final DSC.

In this work, PEs were prepared for DSCs with varying dye loading time i.e. 0, 10, 100 and 1000 minutes. It is commonly known that if the TiO_2 film is not fully dye loaded, the dye concentration is expected to be larger in the outer surface of the TiO_2 film than in the inner parts of the TiO_2 film. When analyzing the results, it is important to keep in mind this uneven distribution of the dye. The electrical performance of the DSCs prepared with PEs with varying dye loading time is shown in the Table 5. The results show that the dye loading is improving the DSC performance till 1000 minutes (approximately 16 hours), however, from this data it is not possible to determine the optimized dye loading time.

Table 5: Performance parameters of the DSCs having sensitization time of 0, 10, 100 and 1000 min respectively, obtained through current voltage curves measured under 1 Sun. Table from Publication IV.

Time (min)	i_{SC} (mA/cm²)	V_{OC} (V)	*FF* (%)	η (%)
0	0.02	0.21	38.5	0.0
10	1.16	0.59	65.9	0.4
100	4.22	0.65	67.9	1.9
1000	10.14	0.72	70.3	5.2

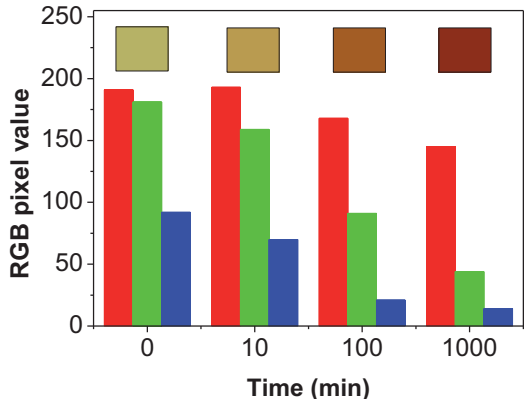

Figure 18. RGB pixel values of the active area of DSCs having different dye loading times. Figure from Publication IV.

For the visual analysis photographs of all the DSCs prepared with varying loading times were taken after the cell assembly. With an increasing dye loading time, the TiO_2 film got darker and darker, and correspondingly the photographs show that the RGB pixel values are also decreasing as shown in the Figure 18. As simultaneous decrease in R, G and B values are occurring; visual analysis can be performed in a better way by monitoring the intensities of the dye color. Therefore, the image processing in gray scale format is more convenient here. For this purpose, the RGB pixel values are transformed to gray scale for all the images using the Eq. 11 [73]:

$$\text{Gray} = (0.299 \times R + 0.587 \times G + 0.114 \times B) \qquad (11)$$

The decreasing gray scale values as shown in Figure 19 and increasing performance as shown in the Table 5 with increasing dye loading time is in a relationship as expected. Therefore, image processing method can be used to monitor the dye loading process as also done in previous studies [41]. More experiments and thorough calibration work is needed to estimate the performance of the DSC using the color of the PE.

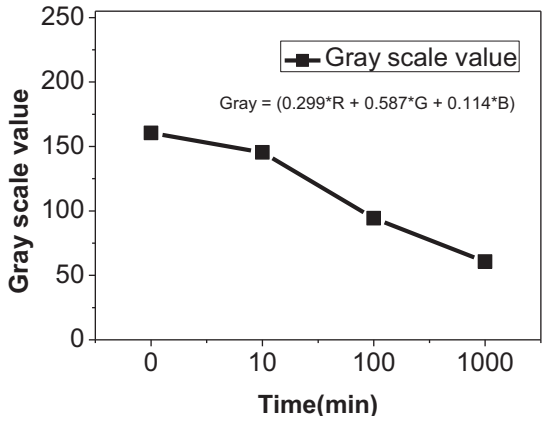

Figure 19. Gray scale value for the corresponding RGB values given in Figure 5 using Eq. 11. Figure from Publication IV.

4.3. Stabilization of flexible metal based DSCs (Publication V & VI)

There is a significant interest for using metal substrates in DSCs due to the feasibility for the roll-to-roll manufacturing. Usage of cheap flexible metal substrate would significantly drop the cost of the DSC as majority of the material cost is due to the TCO coated substrate [10]. One compromise is that the cell is no more bifacial and light harvesting can be done only from one transparent side of DSC. Additionally, attaining long term stability with metal substrates in a DSC is required for their usage in this technology.

4.3.1. Stability of metal photoelectrodes

In order to be used at the PE of DSC, firstly flexible metals need to be chemically stable against the corrosive electrolyte. Secondly, they must withstand the high temperature i.e. approximately 500°C required for the TiO_2 film sintering. Many metals corrode in the iodine electrolyte [24,25]. Basically the lowest cost metal that remained stable after so called electrolyte soaking test is stainless steel (StS) [24,25]. In an earlier study, the stability of wide range of metal substrates as a DSC PE was investigated [74]. In that work, metal substrates such as StS 314 and StS 321, acid proof StS such as StS 316 and StS 316L, Inconel alloy 600 and Titanium foils (Ti) were used as a substrate for PE. Commercially available high stability electrolyte (HSE) by Dyesol and thermally platinized FTO glass as CE were used. The DSCs prepared with above mentioned metals together with a glass reference cell were exposed to light soaking test at 40˚C with a light intensity of 1 Sun.

It was found that all the metal cells degraded completely in a couple of days except the ones prepared with Inconel 600 and Ti. One of the hypotheses was that the degradation was due to corrosion. However, the SEM images did not reveal any corrosion marks [74]. There were also two other hypothesis, increased current leakage and so-called iron contamination, but those were not either supported by the tests. Further research is needed to find out the degradation mechanism leading to this quick failure. On the positive side Inconel 600 and Ti passed the light soaking test and are thus suitable metal substrate materials for the PE of a DSC. The stability results of that study are presented in the Table 6 for the sake of comparison with the metal CE studies (Publication VI).

4.3.2. Stability of metal counter electrodes

In order to be used at CE of DSC, the flexible metals need to be chemically stable as in case of PE. At the CE, the metal substrates do not necessarily have to withstand high temperature treatment depending on the catalyst layer deposition method. For instance, if the CE is thermally platinized then flexible metal must withstand approximately 400°C. However, there are low temperature treatments available to prepare a good quality CE [19,24,26-31]. In Publication V, metal based CEs were prepared using both thermally platinized (high temperature treatment) and sputtered Pt (low temperature treatment) to find the performance and stability of DSCs.

First, the DSCs were prepared with the same selection of metals i.e. StS 304, StS 321, StS 316, StS 316L, Inconel 600 and Ti together with the glass based DSC as reference as used in earlier study [74] using thermal Pt. The cells were tested under the same ageing conditions as for the DSCs with metal based PEs in Section 4.3.1 i.e. under light intensity of 1 Sun at 40°C. Interestingly, the results obtained with the metals at CE were different from the results when same metals were used at the PE as illustrated in Table 6. DSCs with counter electrodes on StS 304, StS 321 and even Inconel, which was stable at PE, degraded overnight. On the positive side, both StS 316 and StS 316L showed better stability at the CE as compared to when used at the PE. In spite of better stability, StS 316 degraded gradually during the first four weeks of ageing followed by a dramatic degradation leading to complete loss of performance. However, some of the StS 316L based cells remained stable throughout the ageing period. Only Ti based cells were consistently stable with the thermal Pt treatment. On the cells that were degraded at the CE (including StS 304, StS 321, StS 316 and Inconel 600), corrosion marks were found on the substrate using SEM and the color of the electrolyte was also bleached. Therefore, it can be concluded that corrosion is the main reason for the failure of the degraded cells when using metals based CE. In contrast such corrosion marks have not been detected in the case of metal based PE [74]. This further confirms that degradation reactions occurring at PE and CE are different. The reason for this is suspected to originate from the different polarization in the case of PE and CE.

To improve the stability of metal based DSCs, a protective coating of sputtered Pt was applied on the metal substrates. The sputtered Pt acted as both the protective layer as well as the catalyst layer. The DSCs were prepared with the same above mentioned metals and subjected to similar testing. Figure 20 shows that the sputtered Pt was successful in preventing corrosion; in all but one case (Inconel), the cells were stable during the 1000 h test. It is evident from the improved stability results that the higher coverage provided by the sputtered Pt to the metal substrates as compared to thermal Pt increased the resistance against the corrosive action of the electrolyte. The degradation of the Inconel 600 even using sputtered Pt showed the tendency of Inconel 600 for the corrosion at the CE. It might be related to the high nickel content (72%) in Inconel 600, as StS were remained stable which have 10% nickel.

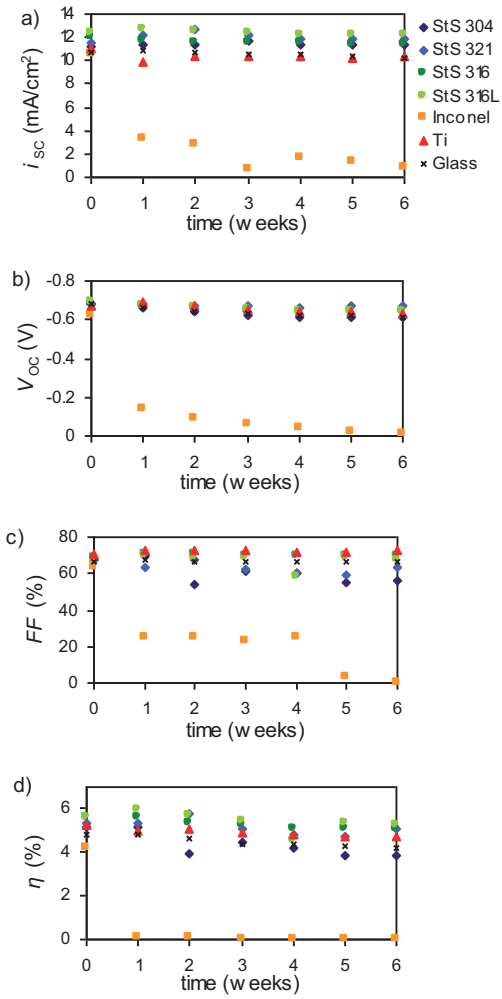

Figure 20. Typical performance parameters of cells with different metals as counter electrode substrate and sputtered Pt catalyst layer a) short circuit current density i_{SC}, b) open circuit voltage V_{OC}, c) fill factor *FF* and d) efficiency η as a function of time. Figure from Publication V.

The degraded Inconel 600 substrate was further investigated using SEM imaging. The image of the Inconel substrate before the ageing test is shown in the Figure 21c. After the ageing test, a number of corrosion pit holes

appeared on its surface as shown in Figure 21a. The Figure 21b showed the magnified image of the pit hole marked with a rectangle in Figure 21a.

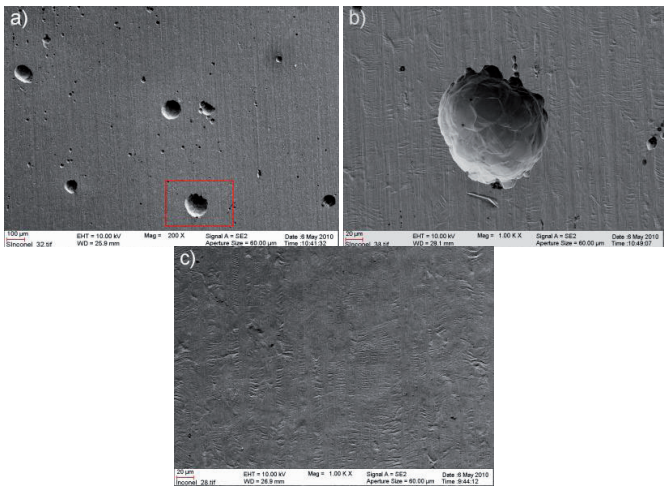

Figure 21. a) A SEM image of a sputtered Inconel 600 substrate after the ageing test. b) A magnified SEM image from the area which is marked with rectangle in figure a showing a corrosion pit hole. c) A SEM image of Inconel substrate before the ageing test. Figure from Publication V.

The EIS was performed on the cells at the open circuit conditions under illumination as the performance of the light independent series connected components such as series resistance R_S and charge transfer resistance R_{CE} at the CE can be quantitatively compared. In the EIS analysis, all the Pt sputtered metal CEs, except Inconel 600, as well as reference glass DSC showed similar trend in ageing. As an example Pt sputtered StS 316 is presented here as shown in

Figure **22**. The Pt sputtered Inconel 600 based DSC degraded before the initial measurement due to corrosion.

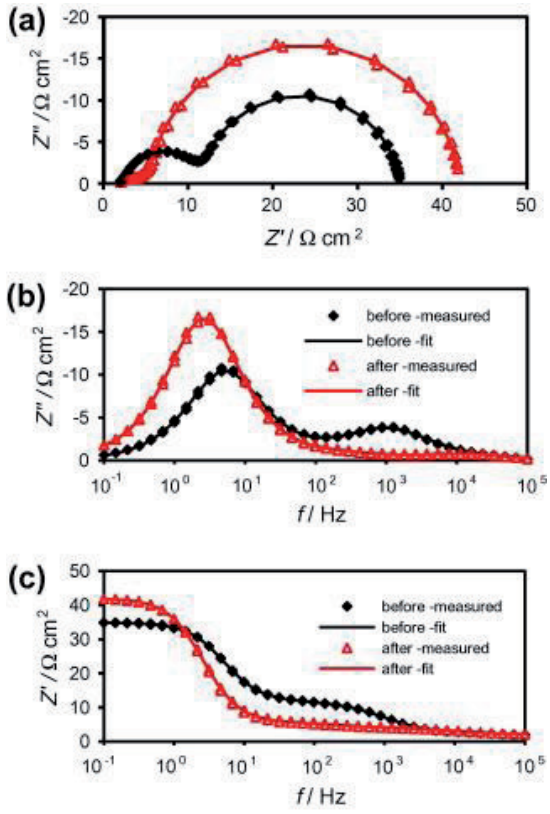

Figure 22. EIS response of a DSC having Pt sputtered StS 316 as counter electrode before and after the light soaking test measured under illumination at open circuit conditions. The data is shown as a) a Nyquist plot b) imaginary impedance *Z"* vs. frequency *f* and c) real impedance *Z'* vs. *f*. Figure from Publication V.

Figure **22**a shows the Nyquist plot of the Pt sputtered StS 316 based DSC measured under illumination at open circuit conditions. The R_S which is mainly caused by the sheet resistance of the substrate and given in the Nyquist plot by the real axis value before the left most semicircle starts. It is clear from

Figure **22**a that R_S did not change during the ageing. The smaller circle at the left in

Figure **22**a, corresponds to the high frequency features in

Figure **22**b&c and represents the R_{CE} at the CE/electrolyte interface. It was found that R_{CE} decreased from 10 Ωcm² to 1.5 Ωcm² which relates to a significant improvement in the catalytic activity at the CE. This increase in the catalytic activity should give rise to improvement in *FF*. However, such increase in *FF* was not detected as Figure 20 indicates. At the same time, a slope (45°) attached to the semicircle appeared in the case of aged DSC as shown in

Figure **22**a. This slope represents the transport resistance in the TiO_2 film. It is not possible to conclude whether the transport resistance increased in the aged cell or not, because the slope was visible in the EIS spectrum before the ageing.

Table 6. A comparison of stability of metal based DSCs when different metals substrates were used at PE and CE under ageing conditions of 1 sun equivalent light intensity at 40 °C for 1000 h test. Stable = passing of 1000 h with only minor loss of performance; unstable = significant loss of performance during 1000 h test; very unstable = significant loss of performance in first 24 h of testing. Table from Publication VI.

	Metal PE	Metal CE with a thermal Pt layer	Metal CE with a sputtered Pt layer
StS 304	very unstable	very unstable	stable
StS 321	very unstable	very unstable	stable
Acid proof steel 316	very unstable	unstable	stable
Acid proof steel 316L	very unstable	stable	stable
Inconel 600	stable	very unstable	unstable
Titanium	stable	stable	stable

Table 6 gives a general overview of the stability of different metal substrates including StS 304, StS 321, StS 316, StS 316L, Inconel 600 and Ti. The stability results are given for metal substrates used at the PE and the CE with thermal Pt or with sputtered Pt. The stability status is defined into three categories i.e. very unstable, unstable and stable. The DSCs which remained stable or lost minor performance over the entire ageing period are declared as stable. Those DSCs which lost their performance significantly during the ageing period are marked as unstable. On the extreme side those cells which degraded completely within 24 hours are marked as very unstable. It is clear from Table 6 that only Inconel 600 and Ti are found stable while the rest of the metals were very unstable when used at the PE. Different results were obtained only for StS 316, StS 316L and Inconel 600 while rest of the results remained the same when the metals were used at the CE using thermal Pt as the catalyst. Inconel 600 was found to be very unstable at the CE. StS 316 was found to be unstable and StS 316L was found to be stable. Dramatic improvement was seen among all the cells when sputtered Pt was used at the metal CE. All the metal based DSCs remained stable in the test with an exception of Inconel 600 which was found unstable but not very unstable. It shows that Inconel is highly prone to corrosion and even the protective sputtered Pt coating did not manage to save it.

4.4. Segmented cell method to study DSCs (Publication VII)

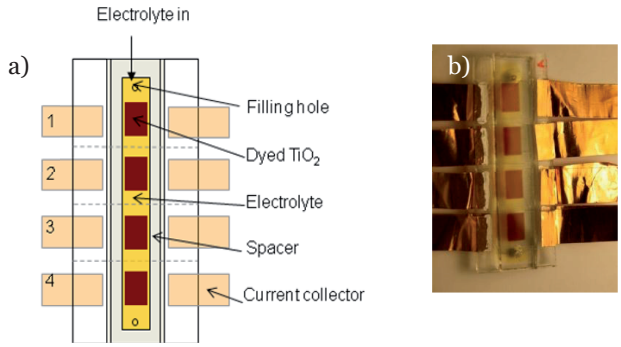

Figure 23. a) Schematics and b) a photo of a four segment cell. Figure from Publication VII.

Recently, it was found that the electrolyte filling process resulted in spatial variation of the electrolyte components in the DSC causing spatial variation in performance [75]. The motivation in this work (Publication VII) was to find which electrolyte components are subject to this effect. The overall aim was to minimize the spatial performance losses which would affect in particular large area cells. For this purpose, a four segmented cell configuration was applied to monitor the performance variations across the cell. The schematic and a photograph of the segmented cell configuration is shown in the Figure 23.

Here five different electrolytes listed in Table 7 were investigated. The composition of electrolytes was chosen in such a way that it allows to observe the effect of each additive or components used in the electrolytes. For instance, the first electrolyte contains TBP and LiI in addition to I_2 in MPN. In second electrolyte the TBP is replaced with NMBI keeping other components the same. In third electrolyte, LiI is replaced with PMII and in fourth electrolyte GuSCN is added to the third electrolyte. Finally, a commercially available electrolyte (HSE by Dyesol) was also used for comparison with other electrolytes.

Table 7. Composition of electrolytes in molar concentrations. Table from Publication VII.

Electrolyte name	I_2	TBP	NMBI	LiI	PMII	GuSCN	Solvent
TBP-LiI	0.05	0.5		0.5			MPN
NMBI-LiI	0.05		0.5	0.5			MPN
NMBI-PMII	0.05		0.5		0.5		MPN
NMBI-PMII-GuSCN	0.05		0.5		0.5	0.1	MPN

The I-V curves of all the cells in the segmented cells were measured under 1 Sun at RT. The performance parameters of all the segments in the segmented cells are given in Table 8. It was found that V_{OC} was systematically decreasing from segment 1 to segment 4 in the case of all the studied electrolytes. The variation of V_{OC} was the largest with 4-tBP-LiI and NMBI-LiI electrolyte in which case there was also systematic increase of i_{SC} from segment 1 to segment 4. Usually, 4-tBP and NMBI are added in the electrolyte to increase the V_{OC}. Thus, decrease in V_{OC} in all the cells results due to decreasing concentration of 4-tBP and NMBI from segment 1 to segment 4. In an early study, electrolyte solution containing only LiI and I_2 gave uniform performance in the 4-segmented cells [75], which means LiI alone does not cause spatial variation problem. However, here LiI is used together with 4-tBP or NMBI. In literature formation of Li^+ and 4-TBP complexes have been reported [76,77]. It appears that in segments having higher concentration of 4-tBP or NMBI, Li^+ concentration decreases due to the complex formation. Decrease in Li^+ concentrations leads to the higher shift in the conduction band of TiO_2 which would result in decrease in injection efficiency and finally result in decreasing i_{SC}.

Table 8. The performance parameters of the individual segments and their parallel connection in comparison to the small reference cell for different electrolytes. Table from Publication VII.

	J_{SC} (mA/cm^2)	V_{OC} (V)	FF (%)	η (%)
4-tBP-LiI				
segment 1	3.09	0.759	72	1.69
segment 2	7.00	0.779	61	3.34
segment 3	9.85	0.717	58	4.09
segment 4	10.15	0.616	57	3.57
parallel connection	7.52	0.698	57	3.00
small reference	9.94	0.731	62	4.52
NMBI-LiI				
segment 1	4.63	0.752	70	2.45
segment 2	8.30	0.762	60	3.82
segment 3	9.40	0.732	55	3.81
segment 4	10.44	0.624	43	2.77
parallel connection	8.19	0.714	51	3.00
small reference	9.70	0.757	61	4.46
NMBI-PMII				
segment 1	8.69	0.758	66	4.33
segment 2	9.29	0.728	65	4.36
segment 3	9.60	0.717	64	4.44
segment 4	8.84	0.717	65	4.15
parallel connection	9.10	0.729	65	4.31
small reference	8.67	0.754	67	4.37
NMBI-PMII-GuSCN				
segment 1	9.17	0.797	66	4.83
segment 2	10.01	0.746	65	4.85
segment 3	10.24	0.721	65	4.78
segment 4	9.26	0.705	64	4.19
parallel connection	9.67	0.739	65	4.62
small reference	10.06	0.768	67	5.19
HSE				
segment 1	9.86	0.743	62	4.54
segment 2	10.61	0.676	64	4.57
segment 3	10.73	0.639	62	4.27
segment 4	10.09	0.642	63	4.05
parallel connection	10.32	0.667	63	4.32
small reference	10.93	0.704	66	5.07

As the hypothesis for the phenomenon is that the electrolyte components are not distributed evenly, the next step was to perform a chemical analysis of the electrolyte in each segment. The Raman spectroscopy for being a non-destructive method was suitable for analyzing different segments in all the segmented cells. However, the FTO-glass plates used in the actual segmented cells were in fact so thick (2.5 mm) that they interfered with the quality of the Raman response. Thus for the Raman cells a series of segmented cells were made in which the counter electrode was replaced with a thin microscope glass (1 mm).

The Raman spectra at the PEs of the reference cells of all the five different electrolytes are shown in the Figure 24. The Raman spectra for all the cells were apparently quite same except at some frequencies the intensities of the peaks are varied. This already implies that there were no separate peaks seen for different electrolyte additives such as TBP and NMBI. In literature, Raman peak for 4-tBP and NMBI should appear at 996 cm^{-1} and around 1360 cm^{-1} respectively [78,79]. However, there were no peaks in those regions showing weak Raman signals for the 4-tBP and NMBI. This might be due to the fact that the sample referred in the literature [78,79] were only based on a mixture of MBI and LiI in MPN or 4-tBP liquid, whereas here the Raman spectroscopy was performed on complete DSCs which also included the dyed TiO_2 films. Other studies using Raman spectroscopy on complete DSC also did not show these peaks either [79,80].

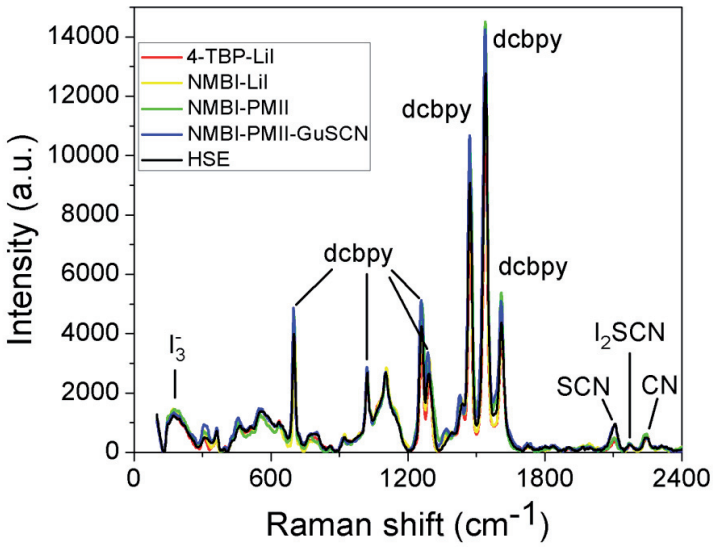

Figure 24. Comparison of Raman spectra at the photoelectrodes of reference cells with the different electrolytes in the range 0-2400 cm^{-1}. Figure from Publication VII.

There were significant differences in the peak heights around 2106 cm^{-1}. The peak around 2106 cm^{-1} is associated with the thiocyanate (SCN^-) in the literature [79,80]. The SCN- ligand which is attached to the Ru atom of the dye plays a major role in regenerating the oxidized dye. In order to see the effect of the spatial distribution of electrolyte on the SCN- ligand attached to the dye in a better way, the Raman spectra of all the segments of the segmented cells and corresponding reference cells are presented in the range of 2000 to 2300 cm^{-1} as shown in the Figure 25.

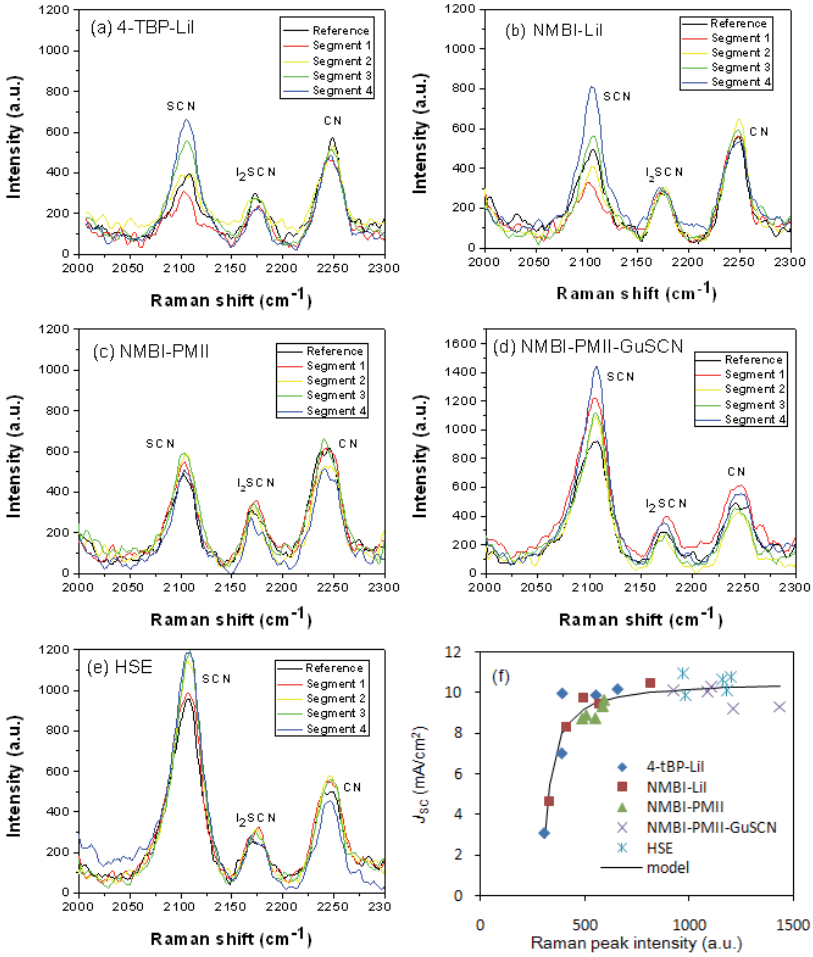

Figure 25. Comparison of Raman spectra at the photoelectrodes of segmented cells and corresponding reference cell using electrolyte a) 4-tBP-LiI, b) NMBI-LiI, c) NMBI-PMII, d) NMBI-PMII-GuSCN and e) HSE in the range of 2000 – 2300 cm^{-1}. f) The SCN$^-$ peak heights of all the segmented and reference cells vs. J_{SC}. The solid line is a phenomenological model fitted to the data: $J_{SC} = J_{MAX}$ $(I-I_0)/[(I-I_0)-R]$ where J_{MAX} is maximum photocurrent expected from the device I_0 is a background SCN$^-$ peak intensity and R is a recombination (or decay) term inhibiting regeneration (or injection). The fit parameters are J_{MAX} = 10.5 mA/cm^2, I_0 = 294 and R = 30.7. Figure from Publication VII.

In the segmented cells with 4-tBP-LiI and NMBI-LiI electrolytes, the height of the SCN^- peaks at 2106 cm^{-1} showed an increasing trend from segment 1 to 4 as shown in Figure 25a and b. Interestingly in these segmented cells, i_{SC} showed a similar increasing trend as given in Table 8. This indicates that there may be a relation with the intensity of the SCN^- in the Raman spectra and i_{SC}. In the literature [79-81], it has been suggested that the differences in the electrolyte composition can cause SCN^- ligand substitution processes and both 4-tBP and NMBI have been reported substituting the SCN^- ligand. In the segments with low i_{SC} and higher V_{OC}, a higher concentration of 4-tBP and NMBI is expected as filtering of those additives in the TiO_2 would have such effects on the photovoltaic performance. Hence, it seems highly probable the SCN^- was exchanged with 4-tBP and/or NMBI. Interestingly, Li^+ has been reported to protect the SCN^- ligand exchange with MBI by forming a complex between Li^+ and MBI [79]. Therefore in the segments containing high concentration of NMBI or 4-tBP with low concentration of Li^+, there would have occurred more SCN^- ligand exchange reactions. When bulky PMI^+ was used instead of small Li^+ in the case of NMBI-PMII electrolyte, there was no significant difference neither in the peak height of SCN^- as shown in Figure 25b&c nor in the i_{SC} values. This implies that the PMI^+ ions protected the SCN^- ligand from the exchange reactions. This result is in accordance with the literature that the bulky ion protects SCN^- ligand better as compared to small Li^+ [79]. The intensity of the SCN^- peak increased significantly in the case of NMBI-PMII-GuSCN (Figure 25d) as compared to the case of NMBI-PMII (Figure 25c) suggesting that GuSCN may act as a source of SCN^- ligand. Similarly in the case of HSE, the intensity of the SCN^- peak was high (Figure 25e) and close to the case of NMBI-PMII-GuSCN (Figure 25d), suggesting that HSE may have contained GuSCN. Interestingly, the i_{SC} values were higher for NMBI-PMII-GuSCN and HSE, and did not change much as compared to the cells without having GuSCN. Therefore, the variation in the intensities of the SCN^- in the Raman spectra (Figure 25) is indeed related to the variations in i_{SC} (Table 8).

Figure 25f i_{SC} of the segmented cells and corresponding reference cells was plotted as a function of Raman peak intensity of the SCN^-. A simple phenomenological model (see Figure 25 caption) is used to fit the i_{SC} data in Figure 25f. In the model the SCN^- peak intensity is assumed to be proportional to the rate of charge separation in the dye molecules which

may be due to dye regeneration and/or electron injection into the TiO_2 conduction band. In addition, this process competes with an approximately constant rate of electron-dye recombination or excited state decay. Indeed, the IPCE data suggested that most likely regeneration and injection efficiency are influenced by the spatial variation of electrolyte components. Therefore, the mechanism affecting the photocurrent is more complex than the simple model presented in the Figure 25 caption. Hence, in order to build a quantitative understanding more detailed measurements of regeneration would be required [81]. Here the purpose of the model is mainly to illustrate trend that the loss of SCN- ligands would have on i_{SC} and that the data agrees with it. Figure 25f shows clearly that below the intensity value of approximately 500 a.u., there is a relation between the i_{SC} and peak height of the SCN^-. It may be concluded that the low i_{SC} in some of the cells may be limited by the low concentration of SCN^- ligand. Furthermore, Figure 25f suggests that at intensities above 500 a.u. i_{SC} is not limited by the concentration of SCN^-.

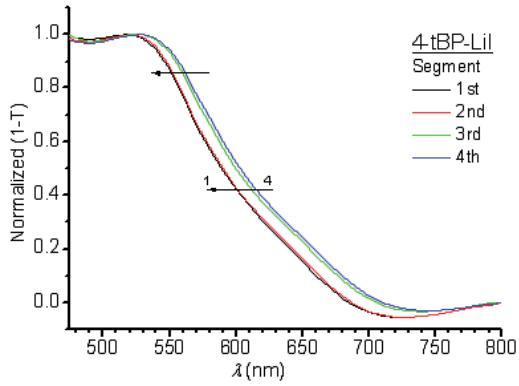

Figure 26. Comparison between the normalized (1-T) for segment 1 to 4 for segmented cell with electrolyte 4-tBP-LiI. The arrows show the blue shift from segment 4 to 1. Figure from Publication VII.

In the transmission (T) measurements, it was found that the spatial distribution of electrolyte components also affects the absorption (1-T) by the cells. As an example absorption data (1-T) of segmented cell with 4-tBP-

LiI electrolyte is presented in Figure 26. The trend in Figure 26 is that the spectra are shifted to the red side from segment 1 to 4. In literature, SCN^- ligands are reported to tune the spectral response of a DSC towards red [62,82]. Therefore, any exchange of SCN^- ligands with the electrolyte additives would cause a blue shift in the cell absorption spectrum. The Figure 26 shows a blue shift in the absorption spectra of the dye which corresponds well with the variation in the peak intensity of the SCN^- shown in Figure 25a. The substitution of the one of the two SCN^- in each N719 dye with 4-tBP would give approximately 30 nm IPCE shift towards blue side (Publication VII). When the transmission and IPCE spectra of all the segments in segmented cell having 4-tBP-LiI were compared, a 15 nm blue in the transmission and a 20 nm blue shift in the IPCE were obtained from segment 4 to segment 1 (Publication VII). Therefore, it can be estimated that approximately about 25% of the SCN^- ligands attached to the Ru atoms in the dye, were substituted in the first segment.

5. Summary and Conclusions

Performance, cost and stability are the fundamental factors affecting the commercialization of DSCs. In addition, the materials and manufacturing methods used for DSCs should be compatible for roll-to-roll production. Degradation of DSCs due to the instability of the materials or due to the manufacturing technique adversely effects their commercialization. Achieving long term stability with cheap materials and easy manufacturing methods using flexible substrates is the prerequisite for success of this technology. This research work investigated the degradation of DSCs, highlighting the key challenges the technology is facing today. The goal of the work was to find more stable materials, improve understanding of their effects on the DSC stability, and develop experimental methods that give improved resolution of the degradation mechanisms.

There are several degradation issues originating from the usage of cheap and flexible materials. Some of the degradation is inherited from the manufacturing processes. New, inexpensive, easy to use and fast methods such as image processing method are useful to study the degradation processes causing a visual change on the appearance of DSC such as bleaching or leakage of the electrolyte. Although many degradation mechanism are occurring at the same time, with the help of the segmented cell method it is possible to separate several degradation mechanism. In addition, it also allows to study the performance degradation due to the spatial variation of the DSC electrolyte. Optical techniques such as Raman spectroscopy and IR spectroscopy were used to detect the chemical changes in the DSCs.

As the purpose of the work was to systematically study the degradation in DSCs, the first step was to perform critical review of the state of the art of stability of DSCs. This resulted in publication I where among other things hypotheses for several degradation mechanisms were collected and

discussed. It was concluded in the review that techniques giving chemical information are very useful to understand the degradation mechanisms. However, mostly the chemical techniques are destructive in nature and cannot be used for in-situ measurements. Information about the chemical changes in the DSCs during the degradation is essential to understand the chemistry inside the DSCs.

One way to detect the chemical changes in DSCs is to link the results obtained from chemical techniques with ones obtained through the standard PV measurements techniques such as I-V measurements under 1 Sun, EIS, IPCE, optical reflectance and transmission measurements. This was the goal of the research reported in publication II. In this publication effects of SCN- ligand substitution reaction, which had been reported in the literature to cause of degradation of DSC at 80°C, was studied in a continued experiment. Using mass spectroscopy analysis it had been shown previously in the literature that SCN ligand of N719 dye can become substituted with tBP at elevated temperatures i.e. 80°C. Here, this substituted compound N719-tBP was synthesized in purpose and used as the sensitizer in DSC, and compared with the cells using pristine N719, to find out the maximum effect of this particular degradation mechanism. The comparative analysis revealed that DSCs based on substituted dye gave 50% less efficiency as compared to the pristine N719 dye based DSCs. IPCE and EIS measurements revealed that the substituted dyes were suffering from lower light harvesting efficiency (30nm blue shift in the absorption spectra as compared to pristine N719), 14% lower charge separation efficiency and 50% shorter electron diffusion length due to lower electron recombination resistance. These results can be used as a finger print of the SCN- ligand substitution reaction occurring in DSCs.

In publication III & IV, the motivation was to correlate the information of chemical changes in DSCs with the visual appearance i.e. color of the DSC which then can further be related to the standard PV measurements. A new in-situ method was introduced in publication III based on the already known image processing techniques. The method was demonstrated to study an important degradation reaction leading to the bleaching of the electrolyte. The yellow color of the electrolyte was first correlated with the RGB values obtained through the image processing method which can be used to estimate the concentration of tri-iodide in the electrolyte. With the

help of this method, it was concluded that the TiO_2 is involved in the electrolyte bleaching reaction under UV+visible illumination at 85°C. It was further checked with standard I-V measurement and the results were in agreement with each other. Later, the image processing method was also demonstrated in publication IV to monitor the dye sensitization process. This method can also be applied to examine the dye degradation since this degradation type changes the color of the dye.

In publication VII, the motivation was to investigate the effect of a manufacturing step used to fill the electrolyte in the DSCs and to find a relationship between the Raman spectroscopy and the other standard PV measurement methods. It was earlier reported that electrolyte filling step causes non-uniform spatial distribution of the electrolyte components leading to the spatial variation in the DSC performance. Recently introduced segmented cell method was used to factor out the electrolyte components vulnerable to spatial variation. Raman spectroscopy was applied together with standard PV techniques to observe the performance degradation in 4-segmented cell. It was found that the nanoporous layer of TiO_2 acts as filter for some additives in the electrolyte resulting in a performance variation. Further, the change in concentration of electrolyte additives 4-tBP, NMBI and LiI affected the substitution of SCN- ligand. When LiI was replaced with PMII, the SCN- ligand was found to be better protected against the substitution reactions. The Raman spectroscopy measurements showed a good relationship between the SCN- peak intensity and the i_{SC} of the DSCs. In worst case, the performance variation was about 35% with conventional electrolyte containing 4-tBp and LiI when the size of the cell was increased from 0.4 cm^2 to 1.6 cm^2. On the other hand, in the best cases the performance variation was about 10% with the electrolyte containing NMBI-PMII-GuSCN when the cell size was increased from 0.4 cm^2 to 1.6cm^2. These findings have important implications on the industrialization of DSCs as there the cell is mostly designed for larger areas where the spatial variation effect due to the molecular filter would be even larger.

In publication V & VI, the motivation was to find a stable TCO free flexible substrate suitable for the roll-to-roll production. In earlier studies a series of cheap metals were tested as a DSC PE. Most of those metals degraded

due to some unknown reason except the Ti and Inconel 600 alloy. Here the same series of metals was tested as the DSC CE using two different methods for the catalyst deposition i.e. thermally platinized and sputter Pt. Most of the thermally platinized cells degraded overnight due to corrosion except Ti and StS 316L. However, all the metal based DSCs i.e. StS 304, StS 321, StS 316, StS 316L and Ti using sputtered Pt remained stable except alloy Inconel 600 which contains 72% of the Ni content. The main conclusion from this study is that there are stable metal alternatives available for both PE and CE applications.

In conclusion, DSCs are facing a lot of challenges on their way for commercialization. There is a need to find stable flexible plastic PE for the DSCs having stable flexible metal CE for achieving completely flexible DSC which is essential for large scale mass production of this technology. In this regard, preparation methods are very important for plastic PE. On the other hand there are also viable metals to be used at PE, however in this case the CE needs to be plastic based. Conventional TCO should be avoided to reduce the costs, therefore alternative transparent conductive materials are needed for plastic substrates. Using plastic substrates brings new severe challenges with respect to sealing due to permeability of impurities like water and oxygen and porosity of substrate. In electrolytes, alternative redox couples should be tested in an effort to improve the stability of DSCs especially in relation to metal substrates. Understanding of degradation mechanisms is essential to improve the stability, hence intensive work is needed to link the chemical changes in the DSCs with the standard PV measurements. Raman spectroscopy, image processing method and segmented cell method can play a significant role in this regard. There is also need to find a viable solution to avoid the spatial distribution of electrolyte in large area DSCs in the future.

References

1. International Energy Agency (IEA), World Energy Outlook (WEO), London 9 November 2010.
2. T. Barker, I. Bashmakov, L. Bernstein, J. E. Bogner, P. R. Bosch, R. Dave, O. R. Davidson, B. S. Fisher, S. Gupta, K. Halsnæs, G.J. Heij, S. Kahn Ribeiro, S. Obayashi, M. D. Levine, D. L. Martino, O. Masera, B. Metz, L. A. Meyer, G.-J. Nabuurs, A. Najam, N. Nakicenovic, H. -H. Rogner, J. Roy, J. Sathaye, R. Schock, P. Shukla, R. E. H. Sims, P. Smith, D. A. Tirpak, D. Urge-Vorsatz, D. Zhou, Technical Summary. In: Climate Change 2007: Mitigation. Contribution of Working Group III to the Fourth Assessment Report of the Intergovernmental Panel on Climate Change [B. Metz, O. R. Davidson, P. R. Bosch, R. Dave, L. A. Meyer (eds)], Cambridge University Press, Cambridge, United Kingdom and New York, NY, USA.
3. European Union Objectives for Energy Technology, SET plan, November 2007.
4. The Energy of Sun, educational website on Astronomy available online at http://www-istp.gsfc.nasa.gov/stargaze/Sun7enrg.htm, quoted 28.09.2011.
5. Discover the True Facts about Solar Energy, available online at http://www.facts-about-solar-energy.com/facts-about-solar-energy.html, quoted 28.09.2011.
6. Solar Energy Could Produce Majority of World's Energy by 2060, available online at http://www.businessinsider.com, quoted 28.09.2011
7. PV status report, JRC European Commission, 2011.
8. Best Research-Cells Efficiencies, National Renewable Energy Laboratory (NREL) website available online at

http://www.nrel.gov/ncpv/images/efficiency_chart.jpg, quoted 05.11.2011.

9. A. Yella, H. Lee, H.N. Tsao, C. Yi, A.K. Chandiran, M. Nazeeruddin, E.W. Diau, C. Yeh, S.M. Zakeeruddin and M. Grätzel, Science, **334**, 629-633, 2011.
10. G. Hashmi, K. Miettunen, T. Peltola, J. Halme, M.I. Asghar, K. Aitola, M. Toivola and P. Lund, Renewable Sustainable Energy Rev., **15**, 3717-3732, 2011.
11. J. Kalowekamo and E. Baker. Sol. Energy, **83**, 1224-1231, 2009.
12. J. Halme, P. Vahermaa, K. Miettunen and P. Lund, Adv. Mater., **22**, E210–E234, 2010.
13. T. Yamaguchi, N. Tobe, D. Matsumoto, T. Nagai and H. Arakawa, Sol. Energy Mater. Sol. Cells, **94**, 812–816, 2010.
14. H. Lindstrom, A. Holmberg, E. Magnusson, L. Malmqvist and A. Hagfeldt, J. Photochem. Photobiol. A, **145**, 107–112, 2001.
15. T.N. Murakami, Y. Kijitori, N. Kawashima and T. Miyasaka, Chem. Lett., **32**, 1076–1077, 2003.
16. H. Pan, S.H. Ko, N. Misra and C.P. Grigoropoulos, Appl. Phys. Lett., **94**, 071117, 2009.
17. K. Miettunen, J. Halme, M. Toivola and P. Lund, J. Phys. Chem. C, **112**, 4011–4017, 2008.
18. J.H. Park, Y. Jun, H. Yun, S. Lee and M.G. Kang, J. Electrochem. Soc., **155**, F145–F149, 2008.
19. S. Ito, et. al., Chem. Commun., **38**, 4004–4006, 2006.
20. K. Kalyanasundaram, Dye-Sensitized Solar Cells, EPFL press, 2010.
21. Y. Bai, Y. M. Cao, J. Zhang, M. Wang, R. Z. Li, P. Wang, S. M. Zakeeruddin and M. Grätzel, Nat. Mater., **7**, 626–630, 2008.
22. D. Kuang, C. Klein, Z. Zhang, S. Ito, J. Moser, S. M. Zakeeruddin and M. Grätzel, Small, **3**, 2094–2102, 2007.
23. D. Shi, N. Pootrakulchote, R. Li, J. Guo, Y. Wang, S. M. Zakeeruddin, M. Grätzel and P. Wang, J. Phys. Chem. C, **112**, 17046–17050, 2008.
24. T. Ma, X. Fang, M. Akiyama, K. Inoue, H. Noma and E. Abe, J. Electroanal. Chem., **574**, 77–83, 2004.
25. X. Fang, T. Ma, M. Akiyama, G. Guan, S. Tsunematsu and E. Abe, Thin Solid Films, **472**, 242–245, 2005.

26. A. Hauch and A. Georg, Electrochim. Acta **46**, 3457-3466, 2001.
27. X. Fang, T. Ma, G. Guan, M. Akiyama, T. Kida and E. Abe, J. Electroanal. Chem., **570**, 257–263, 2004.
28. M.G. Kang, N. Park, K.S. Ryu, S.H. Chang and K. Kim, Sol. Energy Mater. Sol. Cells, **903**, 574–581, 2006.
29. Y. Jun, J. Kim and M.G. Kang, Sol. Energy Mater. Sol. Cells, **91**, 779–784, 2007.
30. S. Kim, Y. Nah, Y. Noh, J. Jo and D. Kim, Electrochim. Acta, **51**, 3814–3819, 2006.
31. J. Nemoto, M. Sakata, T. Hoshi, H. Ueno and M. Kaneko, J. Electroanal. Chem., **599**, 23–30, 2007.
32. J. Chen, K. Li, Y. Luo, X. Guo, D. Li and M. Deng, S. Huang and Q. Meng, Carbon, **47**, 2704–2708, 2009.
33. H.S. Wroblowa and A. Saunders, J. Electroanal. Chem., **42**, 329–346, 1973.
34. F. Fabregat-Santiago, J. Bisquert, G. Garcia-Belmonte, G. Boschloo and A. Hagfeldt, Sol. Energy Mater. Sol. Cells, **87**, 117–131, 2005.
35. J. Bisquert, G. Garcia-Belmonte, F. Fabregat-Santiago, N. S. Ferriols, P. Bogdanoff and E.C. Pereira, J. Phys. Chem. B, **104**, 2287–2298, 2000.
36. F. Fabregat-Santiago, J. Bisquert, E. Palomares, L. Otero, D. Kuang, S.M. Zakeeruddin and M. Grätzel, J. Phys. Chem. C, **111**, 6550–6560, 2007.
37. R. Kern, R. Sastrawan, J. Ferber, R. Stangl and J. Luther, Electrochem. Acta **47** (26), 4213–4225, 2002.
38. C. Kontoyannis, M. Orkoula and P. Koutsoukos, Analyst, **122**, 33–38, 1997.
39. M.J. Pelletier, Appl. Spectrosc., **57**, Number 1, 2003.
40. K. Miettunen, J. Halme and P. Lund, J. Phys. Chem. C, **113**, 10297–10302, 2009.
41. T. Watson, P. Holliman and D. Worsley, J. Mater. Chem., **21**, 4321–4325, 2011.
42. M. Spath, P.M. Sommeling, J.A.M. van Roosmalen, H.J.P. Smit, N.P.G. van der Burg, D.R. Mahieu, N.J. Bakker and J.M. Kroon, Prog. Photovoltaics Res. Appl., **11**, 207–220, 2003.
43. P.M. Sommeling, M. Späth, H.J.P. Smith, N.J. Bakker and J.M. Kroon, J. Photochem. Photobiol. A, **164**, 137–144, 2004.

44. E. Figgemeier and A. Hagfeldt, Int. J. Photoenergy, **6**, 127–140, 2004.
45. M. Ikegami, J. Suzuki, K. Teshima, M. Kawaraya and T. Miyasaka, Sol. Energy Mater. Sol. Cells, **93**, 836–839, 2009.
46. P. Wang, S. M. Zakeeruddin, J. E. Moser, M. K. Nazeeruddin, T. Sekiguchi and M. Grätzel, Nat. Mater., **2**, 402–407, 2003.
47. P. Wang, C. Klein, R. Humphry-Baker, S. M. Zakeeruddin and M. Grätzel, J. Am. Chem. Soc., **127**, 808–809, 2005.
48. P. Wang, C. Klein, R. Humphry-Baker, S. M. Zakeeruddin and M. Grätzel, Appl. Phys. Lett., **86**, 123508, 2005.
49. H.T. Nguyen, H.M. Ta and T. Lund, Sol. Energy Mater. Sol. Cells, **91**, 1934–1942, 2007.
50. P.T. Nguyen, R. Degn, H.T. Nguyen and T. Lund, Sol. Energy Mater. Sol. Cells, **93**, 1939–1945, 2009.
51. E. Palomares, J. N. Clifford, S. A. Haque, T. Lutz and J. R. Durrant, J. Am. Chem. Soc., **125**, 475–482, 2003.
52. A. Kay and M. Grätzel, Chem. Mater., **14**, 2930–2935, 2002.
53. S. Wu, Q. Tai, J. Zhang, S. Xu, C. Zhou, Y. Yang, H. Hu, B. Chen, B. Sebo and X. Zhoa, Nanotechnology, **19**, 215704, 2008.
54. T. Kitamura, K. Okada, H. Matsui and N. Tanebe, J. Sol. Energy Eng., **132**, 2010.
55. W. J. Lee, E. Ramasamy, D. Y. Lee and J. S. Song, Sol. Energy Mater. Sol. Cells, **92**, 814–818, 2008.
56. W. J. Lee, E. Ramasamy, D. Y. Lee and J. S. Song, ACS Appl. Mater. Interfaces, **1**, 1145–1149, 2009.
57. H. Zhu, H. Zeng, V. Subramanian, C. Masarapu, K. H. Hung and B. Wei, Nanotechnology, **19**, 465204, 2008.
58. M.G. Kang, N. Park, K.S. Ryu, S.H. Chang and K. Kim, Sol. Energy Mater. Sol. Cells, **90**, 574–581, 2006.
59. P. M. Sommeling, M. Spath, H. J. P. Smith, N. J. Bakker and J. M. Kroon, J. Photochem. Photobiol. A, **164**, 137–144, 2004.
60. R. Sastrawan, J. Beier, U. Belledin, S. Hemming, A. Hinch, R. Kern, C. Vetter, F.M. Petrat, A. Prodi-Schwab, P. Lechner and W. Hoffmann, Sol. Energy Mater. Sol. Cells, **90**, 1680–1691, 2006.
61. S. Dai, et al., Sol. Energy Mater. Sol. Cells, **85**, 447–455, 2005.

62. M. K. Nazeeruddin, P. Pechy, T. Renouard, S. M. Zakeeruddin, R. Humphry-Baker, P. Comte, P. Liska, L. Cevey, E. Costa, V. Shklover, L. Spiccia, G. B. Deacon, C. A. Bignozzi and M. Grätzel, J. Am. Chem. Soc., **123**, 1613–1624, 2001.
63. S. M. Zakeeruddin, M. K. Nazeeruddin, R. Humphry-Baker, P. Pechy, P. Quagliotto, C. Barolo, G. Viscardi and M. Grätzel, Langmuir, **18**, 952–954, 2002.
64. P. Wang, C. Klein, R. Humphry-Baker, S. M. Zakeeruddin and M. Grätzel, J. Am. Chem. Soc., **127**, 808–809, 2005.
65. D. Kuang, C. Klein, S. Ito, J. Moser, R. Humphry Baker, N. Evans, F. Duriaux, C. Grätzel, S. M. Zakeeruddin and M. Grätzel, Adv. Mater., **19**, 1133–1137, 2007.
66. F. Gao, Y. Wang, J. Zhang, D. Shi, M. Wang, R. Humphry-Baker, P. Wang, S. M. Zakeeruddin and M. Grätzel, Chem. Commun., **23**, 2635–2637, 2008.
67. H. Tian, X. Yang, R. Chen, A. Hagfeldt and L. Sun, Energy Environ. Sci., **2**, 674–677, 2009.
68. B. Macht, M. Turrion, A. Barkschat, P. Salvador, K. Ellmer and H. Tributsch, Sol. Energy Mater. Sol. Cells, **73**, 163–173, 2002.
69. P.M. Sommeling, M. Späth, H.J.P. Smith, N.J. Bakker and J.M. Kroon, J. Photochem. Photobiol. A, **164**, 137–144, 2004.
70. E. Olsen, G. Hagen and S. E. Lindquist, Sol. Energy Mater. Sol. Cells, **63**, 267–273, 2000.
71. N. Papageorgiou, W.F. Maier and M. Grätzel, J. Electrochem. Soc., **144**, 876–884, 1997.
72. H. Nusbaumer, S.M. Zakeeruddin, J.E. Moser and M. Grätzel, Chem. Eur. J., **9**, 3756–3763, 2003.
73. R.C. Gonzalez and R.E. Woods, Digital Image Processing 2nd Edition, 282, 2002.
74. K. Miettunen, X. Ruan, T. Saukkonen, J. Halme, M. Toivola, H. Guangsheng and P. Lund, J. Electrochem. Soc., **157**, B814-B819, 2010.
75. K. Miettunen, J. Halme and P. Lund, Electrochem. Commun., **11**, 25–27, 2009.
76. K. Hara, Y. Dan-oh, C. Kasada, Y. Ohga, A. Shinpo, S. Sadaharu, K. Sayama and H. Arakawa, Langmuir, **20**, 4205–4210, 2005.
77. S. Nakade, T. Kanzaki, W. Kubo, T. Kitamura, Y. Wada and S. Yanagida, J. Phys. Chem. B, **109**, 3480–3487, 2005.

78. C. Shi, S. Dai, K. Wang, X. Pan, F. Kong and L. Hu, Vib. Spectrosc., **39**, 99–105, 2005.
79. H. Greijer Agrell, J. Lindgren and A. Hagfeldt, J. Photochem. Photobiol. A, **164**, 23–27, 2004.
80. H. Greijer, J. Lindgren and A. Hagfeldt, J. Phys. Chem. B, **105**, 6314–6320, 2001.
81. F. Nour-Mohammadi, H. T. Nguyen, G. Boschloo and T. Lund, J. Photochem. Photobiol. A, **187**, 348–355, 2007.
82. Md. K. Nazeeruddin, P. Péchy and M. Grätzel, Chem. Commun., **18**, 1705–1706, 1997.

In the name of Allah, Most Gracious, Most Merciful. Read in the name of your Lord, Who created. Created human, out of a (mere) clot of congealed blood. Read! And thy Lord is Most honourable, He Who taught (the use of) the pen, Taught human that which he knew not. (Holy Quran: Chapter 96, Verses 1-5)

Aalto-DD 53/2012

ISBN 978-952-60-4610-5
ISBN 978-952-60-4611-2 (pdf)
ISSN-L 1799-4934
ISSN 1799-4934
ISSN 1799-4942 (pdf)

Aalto University
School of Science
Department of Applied Physics
www.aalto.fi